Feasibility Evaluation of Sustainable, Green and Rapid-Response Metal-Supported Solid Oxide Cell Technology Integrated with Smart Hydrogen Hub – Final Study Report

Volta Energy Inc.

2024-08-30

Gursaran Singh, Olivera Kesler, Fenglou Zou, and Takis Zourntos

V2.1

This project was supported by the financial contribution of the Independent Electricity System Operator.

This project is supported by the financial contribution of the Independent Electricity System Operator (IESO), through its Hydrogen Innovation Fund. However, the views, opinions and learnings expressed in this report are solely those of the Volta Energy Inc.

Table of Contents

1. Executive Summary

This feasibility study assesses the foundational technologies and associated systems for electric power generation and H_2 fuel production using metal-supported reversible solid oxide cell (SOC) technology. The scope of the study is extensive, spanning the physical design and fabrication of metal-supported solid oxide cell components, the development of dynamic controls for SOC-based stacks incorporating a plurality of cells for interfacing with greater electric power grid and independent system operator, the development of H_2 carrier fuels and decarbonization pathway, and a detailed techno-economic analysis with a fully developed balance-of-plant design, providing rigorously-developed projected net costs of electricity ($[#1]/kW-h) and H_2 ($/kg). Our results combine experimental work on SOC fabrication (electrode development and metal-support construction using novel techniques) and carrier fuel production, mathematical modelling using chemical process methodology and finite element analysis (FEA), and system simulation (using a combination of Matlab/Simscape tools and ASPEN-HYSYS), allowing us to gain insight into several potential applications of interest to the IESO (spanning grid buffering, future EV and fuel-cell EV charging/filling stations, microgrid architecture, and more).

We have achieved the following results with respect to our Quantifiable Outcomes:

1. Ni_3Sn based electrode fabrication with negligible amount of nickel (Ni). (The reason for the different composition than expected has been traced to the need to outsource the coatings to an industrial vendor because the local facility closed for approximately 8.5 months for renovations that lasted longer than expected. The vendor that produced the coatings did not use the same solution composition that we did which corrects for differences in deposition efficiencies between the Ni and Sn ions. Therefore, the coatings had both Ni_3Sn and Ni).
2. Ni_3Sn based electrode with optimized microstructure (porosity volume achieved within target range, between 25% and 45%).
3. Ni_3Sn based fuel electrode stability in CH_4/CO environments for 1,000 hours compared to Ni based fuel electrode **(achieved 18.6%, slightly above our 15% mass target).**

[#1] All costs are presented in CAD unless otherwise specified.

4. Develop and characterize aqueous slurry for fabrication of porous metal structure. (Slurry stability was characterized by settling time rather than zeta potential due to the high solid loading used to obtain good tape casting suitability, which makes zeta potential measurements invalid in that high concentration range. Based on the extremely low setting rate (<1 mm clear solution at the top of column of liquid approximately 46 mm high after 4 hours), the stability of the suspension was excellent, as further confirmed via tape casting.)
5. Development of bespoke fabrication method for porous metal supports based on tape casting. (Low curvature was achieved based on visual inspection. No large surface pores above 40 micrometers were observed in the SEM cross-sections)
6. Characterized metal supports for oxidation resistance and gas permeability. (A 38.6% loss in permeability was achieved after 24 hours of oxidation at 900 °C. The oxide layer that formed under these conditions was approximately 2 micrometers in thickness. This scale of oxide thickness leaves most of the larger pores essentially unaffected, but it has a disproportionate impact on those regions where there are narrow connections between adjacent pores affecting the permeability.)
7. Power grid command response time (achieved response times less than 1 second in simulation for SOFC and SOEC modes, well below the expected 3-second target). Section 4.2 of this report elaborates on the system response and reversibility.
8. SOC power output overshoot (achieved less than 1% overshoot in simulation of controlled SOC responses)
9. GHG Emission Reduction/Decarbonization Potential Quantified (1.37 tonnes of captured CO_2 are utilized for every tonne of methanol produced through either direct CO_2 hydrogenation or syngas pathway, and 2.74 tonnes of captured CO_2 are utilized for every tonne of CH_4 produced. Here, we assume that 100% conversion of CO_2 and 100% selectivity of the intended products, close to current industrial production standards.)
10. The combination of technologies, centered around the SOC, being developed by Volta Energy in this project, can support the electric grid by converting chemical energy in H_2 and H_2 carrier fuels into electricity, as demonstrated in Section 3.3.

2. Introduction and Goal

With the global trend toward decarbonization, Ontario's electric power grid is undergoing a massive transformation. The increased adoption of electrified machinery and heat sources by industry, the proliferation of high-demand electric vehicle (EV) charging stations, and an increase in distribution-side power generation and storage, all contribute to the increasing complexity of the power grid. In addition, the rise of renewable energy, growing presence of microgrids and H_2 electrolysers, will amplify the dynamic nature of the electric power infrastructure, placing the overall reliability of electricity in Ontario at risk.

The use of H_2 as a fuel for electricity production and as a means of energy storage, can make considerable sense from both a performance and cost standpoint. When combined with solid oxide fuel cell (SOFC), solid oxide electrolysis cell (SOEC) or reversible SOC (RSOC) technology, H_2 has the potential to provide rapid response to changes in electricity demand (as rapidly as several tenths of a second), providing excellent power grid buffering and a natural complement to renewable energy sources, and an economical means of energy storage, allowing MWh or even GWh of energy to be cheaply and compactly stored, providing Ontarians with grid buffering and power backup that can last for hours or days.

This feasibility study investigates a special class of SOC technology, namely, that of metal-supported reversible SOCs (MSRSOC), developed by Prof. Olivera Kesler and her team at the Fuel Cell Materials and Manufacturing Laboratory (FCMML), University of Toronto. This promising technology has already been demonstrated to offer excellent cell performance and increased resilience to thermal fluctuation. It offers one of the best options for building long-lasting high performance fuel cell (FC) and electrolysis cell (EC) stacks comprised of thousands of cells (and delivering kilowatts of power). Our work develops the MSRSOC technology and manufacturing methodology while also extrapolating the MSRSOC functionality in simulation to the stack and system level, where its performance within the power grid can be simulated and assessed, and the economic impacts of the full-fledged MSRSOC stacks can be precisely quantified.

As outlined in our original proposal, this study undertook the following activities:

1. Fabrication of an SOC electrode that can function with a diverse set of fuels without impacting efficiency, performance, and durability.
2. Fabrication of an SOC metal support that can withstand the rigors of rapid response to control signals.
3. Smart Hydrogen Hub (SH2) Development: MSRSOC modeling (lumped-parameter and FEA) and model verification, control design for an associated stack or system of stacks, and IESO dispatch response.
4. Hydrogen Gas Conversion/Techno-Economic Modeling/Decarbonization Potential Study.

5. Analysis and Reporting.

3. Approach/Methodology and Assumptions

This section describes our approach to each of the activities listed above, namely: electrode fabrication, metal support fabrication, SH2 development, H_2 conversion/techno-economic, carrier fuel pathways and decarbonization. These various activities are described below, in corresponding sections. **Figure 1** depicts the project landscape around the MSRSOC System.

Figure 1 | RSOC Project Landscape

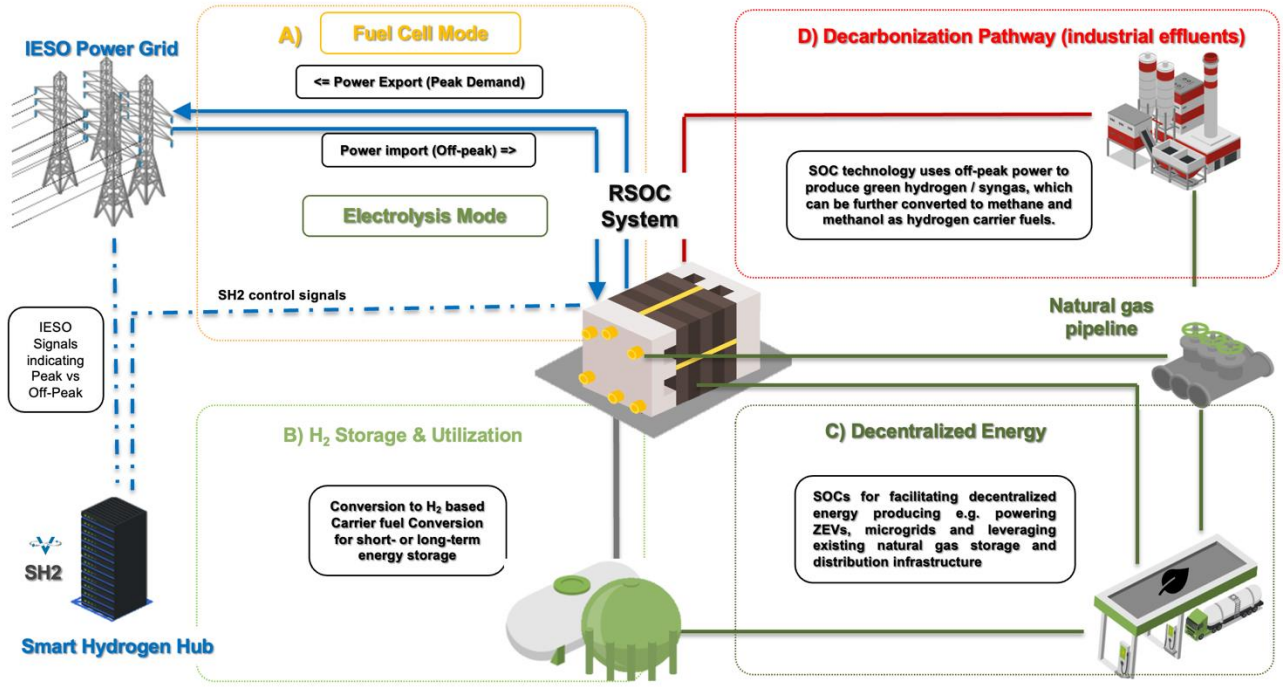

Please note that the appendix sections of this report have detailed reference lists. Some of the important references have been listed in this document as well.

3.1 SOC Technology

3.1.1 Electrode Fabrication

Solution Precursor Plasma Spray (SPPS) is an advanced coating technique where a solution of dissolved precursor materials is injected into a high-temperature plasma jet. The solution is atomized into fine droplets, which rapidly evaporate, decompose, and react in the plasma. The resulting fine particles are accelerated towards the substrate, forming a dense, uniform coating upon impact. SPPS allows precise control over the composition and microstructure of the

coatings, making it suitable for producing high-performance ceramic and metallic coatings with applications in thermal barriers, corrosion resistance, and functional surfaces in various industries [1]. To fabricate SOC electrodes, additional pore former can be introduced to increase porosity for better mass transport and reaction sites compared to thermal barrier coatings, but the fundamental principle is the same. For this study, we fabricated the carbon-resistant Ni_3Sn layer using this method on a dense plate to expose it to dry CH_4 for 1000 hours. There was no electrical current delivering oxide ions to react with deposited carbon and no reaction producing steam to remove the carbon atoms deposited at reaction sites. We observed the deposited layer structure and phase after the exposure to understand if cells can idle in dry CH_4 at operational temperatures.

3.1.2 Metal-Support Fabrication

Sintering strategy

To mitigate the stainless-steel oxidation problem, it is important to reduce the support's surface area to volume ratio by using large steel particles. However, this often introduces large open pores at the surface, making the deposited layers by plasma spray defective with discontinuous electrolytes. Fine steel particles provide a smooth surface for plasma spraying, but the fine porosities fill with oxide quickly. One existing solution is implementing a double-layer structure with a top thin layer fabricated from fine stainless-steel particles and a bottom bulk layer made from large stainless-steel particles by die pressing [2]. This method reduces the impact of fine particle oxidation but does not solve it. Further protection from oxidation or interdiffusion with the electrode can be achieved by applying additional coatings on material surfaces [3],[4].

For porous substrates with small fine porosity, the high surface area increases the consumption rate of chromium, and the small thickness of solid between the small fine pores can prevent the chromium solid state diffusion within the material from being sufficient to replace the consumed chromium, as the reservoir of chromium supplying the nearby surfaces would be rapidly depleted. Sebastian Molin et al. [5] reported very different oxidation behaviours of porous 430 stainless steel sintered below 1100 ^{o}C from dense steel, and they did not try to sinter the substrates to a denser state.

Tape casting

To fabricate SOFC stainless steel substrates, tape casting offers the advantage of producing material in a thin sheet format with the ability to control the thickness and final product size while maintaining high consistency of material properties at low cost [6]. These advantages are even more prominent than the die-pressing method, another common fabrication method for SOC supports [7]. The substrate fabrication is a distinct step from cell layer fabrication, adding additional time to the process. But overall, a single tape casting and firing step for the substrate with three additional plasma spraying steps takes less time than multiple tape casting or screen-printing steps followed by additional firing steps to make all the substrate and cell layers.

Tape casting starts by mixing the powder with a binder solution and other additives, such as a defoamer, plasticizer, dispersant, and thickener. The binder and plasticizer provide the tape

with sufficient strength for further shaping processes, while the dispersant prevents agglomerate formation, and the thickener increases viscosity to stabilize the slurry [8]. The mixed slurry is typically de-gassed in a vacuum before the casting step to prevent pinholes in the cast tape. The tape is cast by passing the slurry under a blade, whose height controls the thickness. The casting surface supports the tape until the slurry dries. A common commercial option for the casting surface is Mylar film, often used on a conveyor and usually coated with silicone. Such an option is often used with organic slurry systems with short drying times. After the solvent fully evaporates, the tape can be peeled off from the casting surface for its intended uses [9].

When fabricating substrates for SOCs, additional porosity is introduced by pre-mixing steel powder with other particles as pore formers in the slurry formation stage. The particles are later eliminated in subsequent thermal treatments and leave the tape in gas form, creating voids where they were located [10]. The porosity volume fraction is crucial to SOC performance, as low gas permeability limits available reactant concentration at the electrodes, thus constraining the power output. To make the substrate compatible with the plasma spraying method, Metcalfe [11] reported that fine steel particles are required to prevent defects on the deposited layers, but this comes at the cost of fast substrate oxidation.

Among tape casting methods reported in the literature, organic solvent-based recipes are used more frequently for fast drying and better-quality control than aqueous recipes. However, the aqueous slip has the advantages of nonflammability, non-toxicity, no solvent recycling being required, and lower cost [7],[12]. It is still necessary to investigate strategies to mitigate or overcome the disadvantages of the aqueous recipe.

The difficulty of low volatility is magnified when combined with thick casting, which is required to obtain sufficient mechanical strength as a SOC substrate. Chang et al. [13] reported thick slip casting with metal powder in a mould, while Mercadelli et al. [6] and Roosen et al. [14] provided organic solvent-based recipes for porous and dense substrates, respectively. Scheithauer et al. [15] reported a procedure for dense aqueous stainless steel tape casting, which is not intended for SOC application.

Freeze casting

A Peltier plate-based freezer was designed for this study, as shown in **Figure 2**. This freezer uses a thermoelectrical cooler to cool down the slurry. The Peltier plate (Laird Thermal Systems, CP2-127-06-L1EP-W4.5) used for this study is 62 mm x 62 mm and, according to the manufacturer's data, can pump heat from the cold side at 70 W when the temperature difference is 30 °C. This plate’s hot side is attached to a circular aluminum sink (PADLED-13080), with fins arranged in a radial direction. This heat sink has a diameter larger than the inner diameter of the Helmholtz coil for magnetic field generation, so the size has been reduced by using a lathe to remove the outer material. Before the machining, epoxy fillers were used to fill in the gap between the fins to prevent the fins from deforming during the machining process.

Figure 2 | Freezer cross-section view

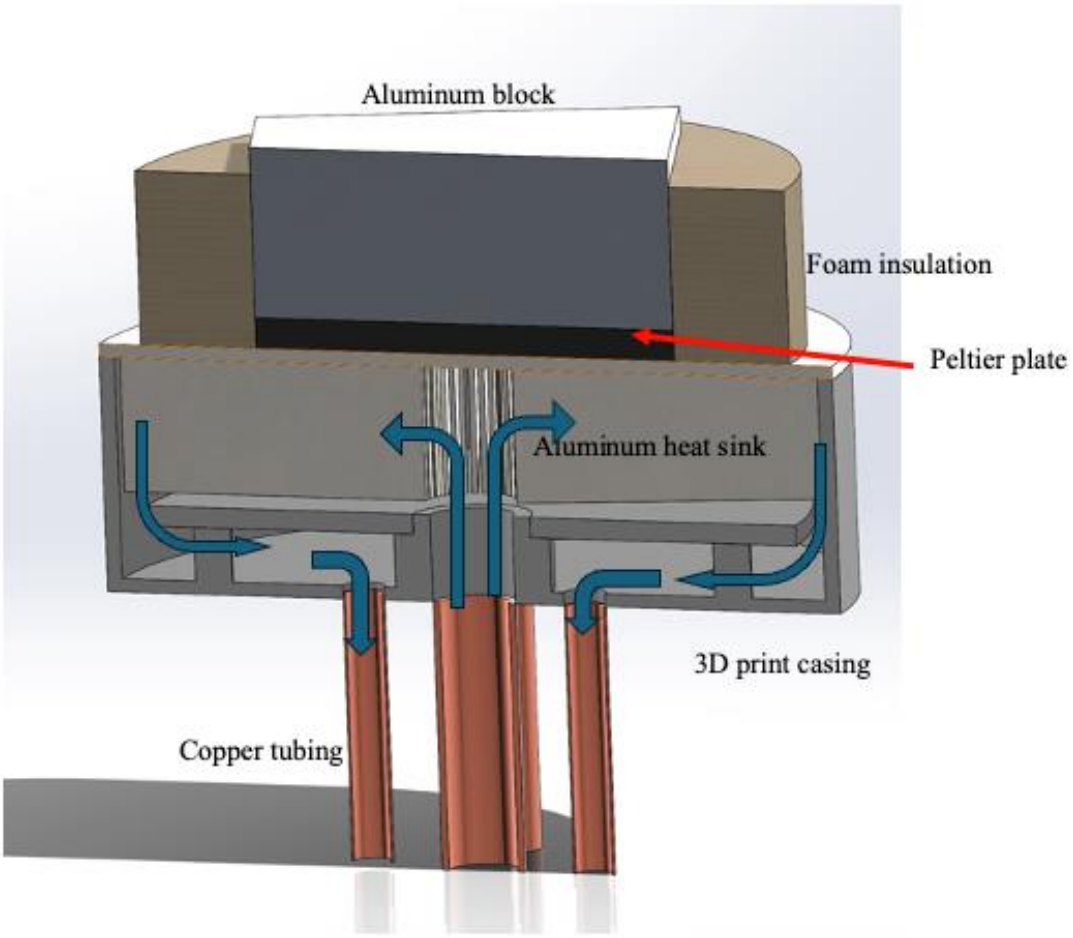

Freezer 3D model cross-section view. The Peltier plate was sandwiched between an aluminum block and an aluminum heat sink. Water was the coolant, flowing radially through the sink.

Magnetic field generation

The Helmholtz coil used for this study was designed according to the guidelines presented in Jake Abbott's work [16]. It was designed to generate a 10 mT magnetic field at a current of 8.25 A. **Table 1** provides more detailed coil parameters, and **Figure 3** defines the geometry parameters.

Figure 3| Geometry parameter definitions

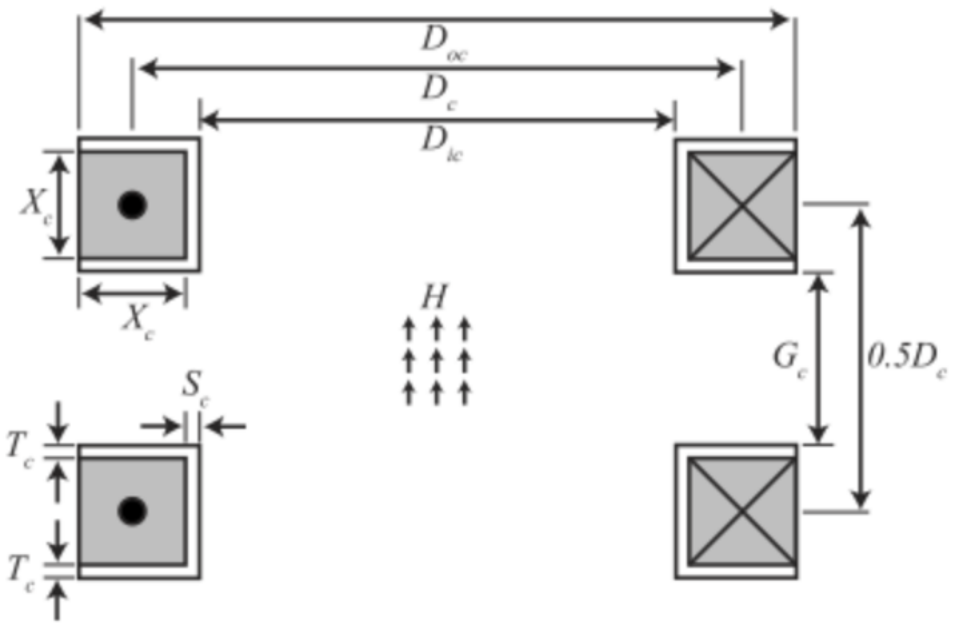

Geometry parameter definitions for circular Helmholtz coil. Image reproduced from [16].

Table 1 | The Helmholtz coil parameters were designed for this study. The parameter definitions can be found in Figure 3.

Wire	X_c	W_{ic}	W_c	G_c	Wire length	Power	Current density
12 AWG	24 mm	115 mm	152 mm	34 mm	106.7 m	37 W	2500000 A/m^2

An aluminum tube with an outer diameter of 115 mm was used as the coil spool. As illustrated in **Figure 4**, this tube had a through cut at the center to allow the insertion of materials. The coils were constrained by 8 half-annular aluminum plates. This coil pair had an inner diameter that could fit outside the freezing bed mentioned above, as shown in **Figure 4**, where the freezing bed top was located at the center plane of the coil pair. When performing the freeze casting experiments, the magnetic field strength can be adjusted by a DC power supply to the coil.

Figure 4 | Magnetic coil and freeze bed assembly

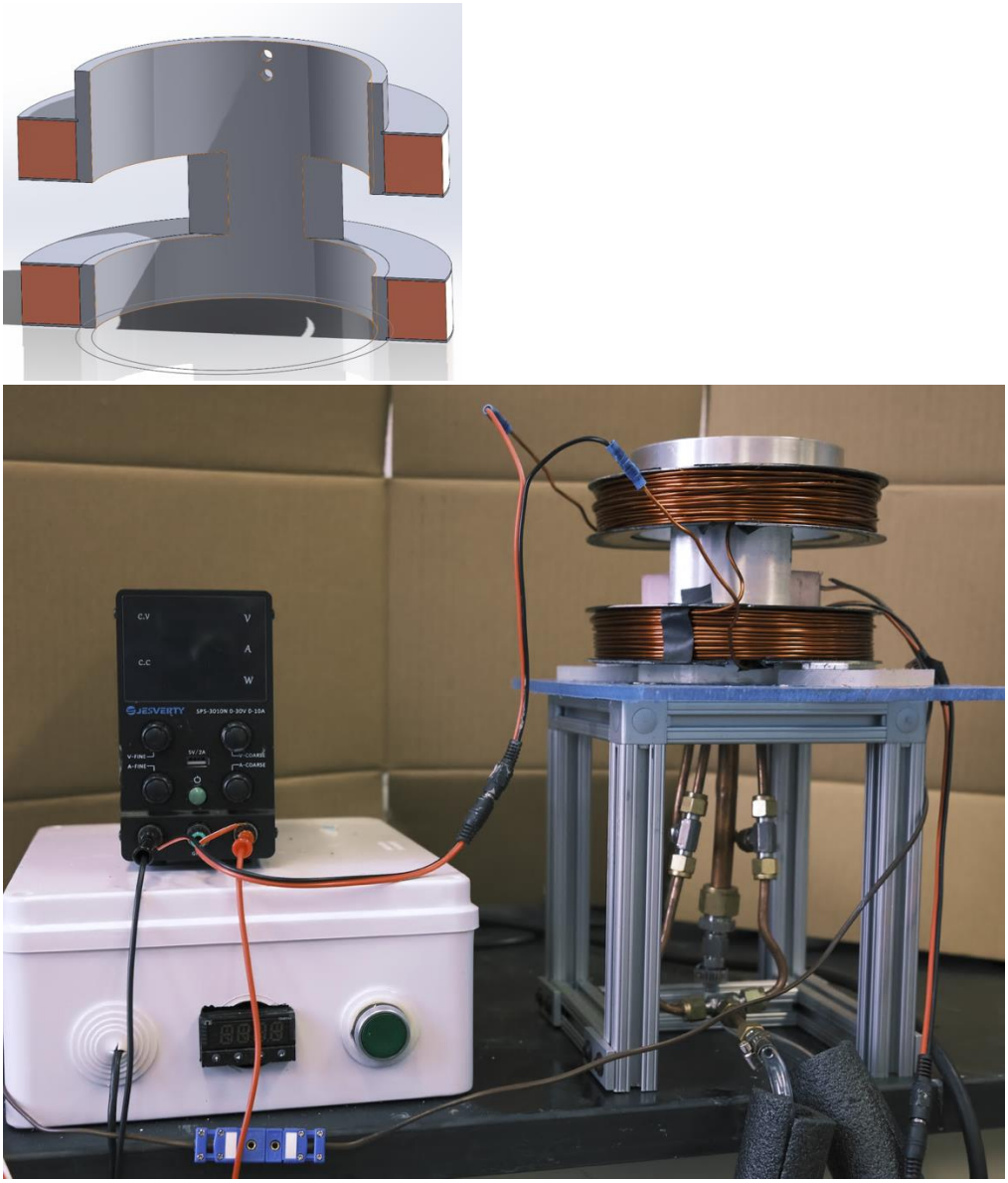

Cross-section view of the designed Helmholtz coil model (top) and the assembled coil with the freezing bed at the center (bottom). The top of the freezing bed has the height to reach the center plane between the two coils. The current going through the coil was controlled by a DC power supply.

A pair of 66 mm diameter and 3 mm thick sintered permanent neodymium magnets (N52) plates were used during the magnetic slip casting process, as shown in **Figure 5**. This setup was designed to generate a uniform magnetic field similar to a Helmholtz coil but uses NdFeB magnets. The Nd magnets, placed on either side, create the magnetic field. Multiple layers of aluminum and acrylic plates/bars support them. The lower magnet is covered by a 1.58 mm thick aluminum plate bonded by thermal glue to a benchtop, allowing easy sample removal. The space between the magnets can be controlled by placing multiple layers of 6.35 mm thick

acrylic plates and aluminum bars to separate the pair of magnets. The upper aluminum bar, with a thickness of 3.16 mm, compensated for the slurry thickness so that the distances from the slurry to the magnets were about the same on both sides.

Figure 5 | Schematic diagram of slip casting fixture

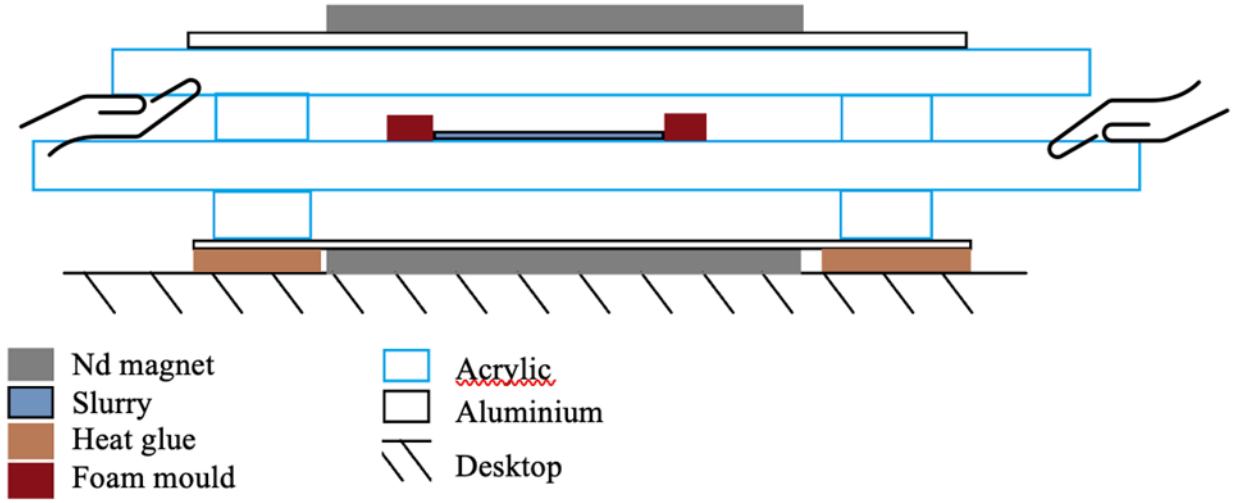

Two magnet plates are kept separate by stacking acrylic and aluminum plates, while the slurry and mould are located at the centre plane between the magnets.

Substrate sintering

Thermal gravimetric analysis experiments (TA instruments SDT Q600) were performed to determine the pyrolysis temperature profile in the intermediate-temperature furnace with a ramp rate of 2 °C/min. The pyrolysis profile of steel powder and organic content in the air was obtained to determine the outgassing temperature and the temperature to switch from air to H_2 for oxidization prevention.

The green tapes were placed on alumina plates, and the organic contents were burned out in an intermediate-temperature tube furnace (Thermolyne 79325, Thermo Fisher).

The final sintering step was carried out in a tube furnace (1632 12HT, CM Furnaces Inc, Bloomfield, USA) filled with pure H_2 (99.99999%) from an electrolyzer (H2-800, Parker Balston) at 100 SCCM for various sintering times ranging from 2 to 6 hours and temperatures from 1100 °C to 1280 °C. Alumina plates were used as the carrying supports during thermal treatments.

Substrate structural property evaluation

The substrate evaluation used five methods: linear size reduction for shrinkage, image analysis for porosity and determination of porosity perimeter to steel area ratio to measure surface area to volume ratio for oxidation resistance, gas permeability, surface profilometry, and accelerated oxidation testing. Shrinkage helps determine the dimensional stability of the substrates during the sintering process, which is crucial for maintaining the structural integrity of the cells. The

image analysis provides a detailed quantitative assessment of the porosity distribution within the substrates, which directly impacts gas permeability and oxidation resistance. The porosity perimeter to steel area ratio helps understand the pores' structural connectivity and correlation with mechanical properties, gas flow, and oxidation behaviour. Gas permeability directly evaluates the rate of gas flow through porous substrates, a critical parameter for the performance of solid oxide cells. The surface profilometry technique assesses the surface roughness, which can affect the bonding and interaction between the substrate and other layers in the cell.

Substrate mechanical property evaluation

Three-point bending (TPB) tests were conducted on a three-point bending stage with a 20 mm span. A computerized Instron 8801 system controlled the motion. The cross-head speed was set as 0.2 mm/min for three-point bending tests following ASTM D760. The hardness was measured by Vicker's indentation using a Buehler micro-hardness tester at a load of 500 g force and load time of 15 s. Three samples of each microstructure type were tested to determine the variability in the mechanical properties.

To prepare the samples for image analysis, the specimens were mounted in epoxy, sanded, and polished with fine diamond paste fine to 1 μm. Etching was done with HF-HNO_3 solution for 4 minutes to observe the grain structure. Both optical microscopy (Axio Scope, Carl Zeiss) and scanning electron microscopy (JSM-6380LV, JEOL) were used to examine the sample structure. Porosity was determined by image analysis using ImageJ software to count the area fraction of dark pixels over the total image area. Electron backscatter diffraction (EBSD) scans were collected using Oxford integrated AZtecHKL advanced software. X-ray photoelectron spectroscopy (XPS, K-Alpha XPS system, Thermo Fisher) measured residue carbon on green tape after outgassing. The samples were prepared by ion milling to remove contamination from the air.

3.2 Smart-Hydrogen Hub (SH2) Development

The Smart-Hydrogen Hub (SH2) sub-system comprises the control system for SOFC and SOEC operation, and an interface for communications with IESO servers (for dispatch signal processing and any necessary requests). In addition, part of our SH2 work necessitates the development of a numerical or "digital" model of SOC functioning, for integration into current and future simulation of fully-fledged SOC control systems, and possibly the optimization of SOC technology itself.

Our control system methodology for the purposes of this feasibility study adhered to a straightforward approach of gain scheduling with linear state feedback control, in which the nonlinear state-space (ODE) model of the SOC was linearized at various points along the power curve of the device (experimentally derived). The linearized system and optimized controller parameters were stored for these discrete power points. Controller selection was based on the power level of the system. Matlab, Simulink and Simscape numerical simulation software were used to develop the complete control systems with process-control-theory-derived ODE models of the SOC in either fuel cell or electrolysis cell modes used as "plants" and state-feedback controllers developed using either eigenvalue placement or linear-quadratic regulator techniques.

For SOC cell models which are as realistic as possible, finite-element analysis (FEA) in the form of COMSOL multi-physics structures were created. Some model verification was carried out using steady-state simulation as well as dynamic simulation in SOC electrolysis mode.

3.2.1 Electro-chemical Process Modelling

The solid oxide cell is depicted as shown in **Figure 6**, with both modes, namely, fuel cell (FC) mode and electrolysis cell (EC) mode, overlaid. In fuel cell mode, H_2 and O_2 gases enter the cell from the upper and lower electrode channels, respectively. The product gas, H_2O, exits the top electrode along with any unreacted fuel (H_2). At the same time, an electrical current is produced which feeds an external load. In EC mode, gaseous H_2O and electrical current are supplied, with the products being O_2 and H_2.

Figure 6 | Solid Oxide Cell

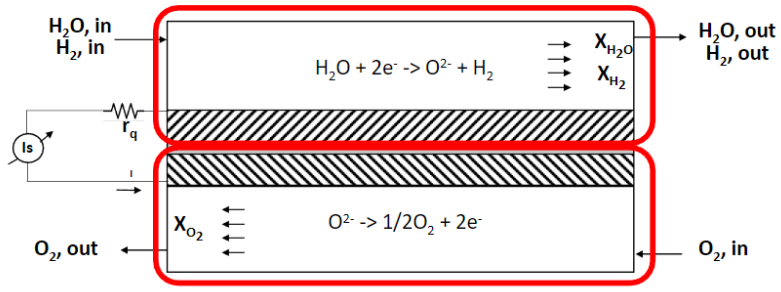

Using mass balances with known reactant and product flow rates (in the case of an SOC, all species are in the gaseous state), a set of ODEs can be derived for FC mode and for EC mode.

These are shown in Appendix 2, as Equations (25)-(28) for FC mode, and Equations (55)-(59) for EC mode.

Derivations as well as model verification were carried out and the methodologies are described in Appendix 2.

3.2.2 Controller Design

The derived models are nonlinear, owing to the Nernst equation and bilinear input (flow rate) and state terms, and contain multiple equilibrium points. Equilibria corresponding to various discrete power points (P_0, P_1, P_2, and so on) along the V-I and power curve shown conceptually below in **Figure 7** (and using actual experimental data in Appendix 2) with pre-selected discrete power "equilibria", are computed, and form the basis of our gain-scheduled approach to controller design. For each equilibrium point, a linearized version of the nonlinear state model is computed. A state-feedback controller is determined using eigenvalue placement of the closed-loop dynamics. Depending on the system state during operation, the closest pre-calculated controller is selected. Therefore, a feedback controller across the entire operational range of the fuel cell can be determined.

Figure 7 | Conceptual V-I Curve for SOC with Power Linearization Points Indicated

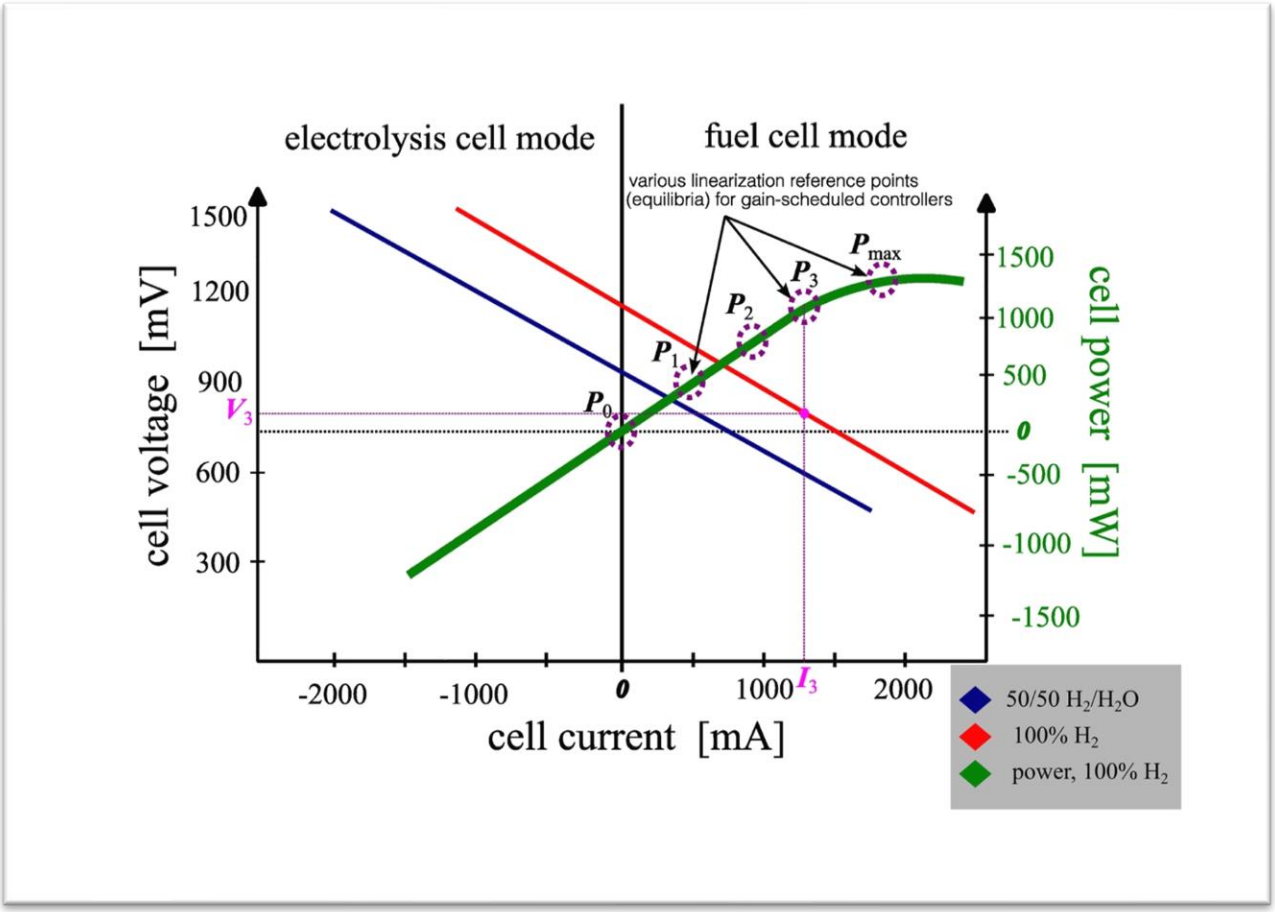

Details of the controller design, including the derivation of state feedback gains and controller topologies, are outlined in Appendix 2. Communication with IESO servers, which would be an essential part of an actual SH2 implementation, were developed for our simulation on a case-by-case basis and as idealized "reference commands" or step function inputs indicating various desired changes in power level or H_2 production. Please see Appendix 2 for details.

3.3 Carrier Fuel Pathways and Decarbonization

The study on H_2 storage and transportation is based on the unique properties of H_2 and an extensive review of the existing literature. For the decarbonization pathway, the approach builds upon the insights from the H_2 storage and transportation study, leveraging the advantages of the developed SOC technology to produce green H_2 gas. Theoretical calculations, supported by HYSYS, are employed to assess energy conversion efficiency and utilized amount of CO_2. This evaluation assumes the availability of captured CO_2.

A comprehensive literature research on catalysts for methanation and methanol synthesis provides a target and framework for developing new catalysts for H_2 conversion into its carrier fuels, utilizing captured CO_2 and contributing to decarbonization pathways. The development of these catalysts fully leverages researcher's experience in catalyst design, knowledge of the catalytic reaction mechanisms, and scientific hypotheses. Detailed characterization of the resulting catalysts is used to further refine the catalyst synthesis. Catalysts are evaluated through conversion reactions, and comparisons of XPS analyses of the catalysts before and after reactions are used to further modify the catalysts, ensuring high catalytic activity and efficiency for H_2 conversion and decarbonization.

As a part of this project, we have studied decarbonization pathways, two of which are CO_2 methanation and CH_4 pyrolysis.

Through the methanation, CH_4 gas is formed from captured CO_2 and green H_2 ($CO_2 + 4H_2 \rightarrow CH_4 + 2H_2O$) produced from water hydrolysis ($2H_2O \rightarrow 2H_2 + O_2$), facilitated by reversible-SOC (r-SOC) using renewable energy or excess electricity from the grid. Through the pyrolysis, CH_4 is converted back to H_2 gas in addition to high-value solid carbon nanotubes ($CH_4 \rightarrow 2H_2 + C$) with zero direct CO_2 emission, as detailed in Appendix 3.

On the other hand, the produced H_2 gas and CH_4 can be used as fuel for r-SOC (SOFC) to generate electricity for the grid when needed. When the grid does not require additional electricity, the produced CH_4 can be stored and transported using existing Natural Gas pipeline for short-term storage, transformed to LNG for short-term storage and easy transportation, or stored underground for long-term storage, as described in Appendix 3.

As also mentioned in Appendix 3, converting H_2 gas to CH_4 has a high energy conversion efficiency (82%), with the added benefit of utilizing captured CO_2. CH_4 pyrolysis is an endothermic reaction; at 500 °C, the process using the catalyst developed by Volta Energy can produce two moles of H_2 gas and one mole of carbon nanomaterial from one mole of CH_4.

When integrated with r-SOC technology, part of the heat released from the SOFC processes can be utilized for CH_4 pyrolysis, thus energy is recycled and used.

Figure 8 illustrates and summarizes the integrated H_2 hubs, long-term storage of H_2, site-specific conversion to H_2 ($CH_4 \rightarrow 2H_2 + C$), as described above. The integrated system will sustain and leverage grid demand and supply. Moreover, the produced carbon nanotubes are very valuable materials, at 75-300 USD/g. Theoretically, 3 kg of carbon nanotubes are produced per kg of produced H_2 gas, assuming 100% CH_4 pyrolysis efficiency. Thus, the entire integrated process is favourable in terms of both energy efficiency and economic viability. For industrial applications, it is essential to separate the produced carbon nanotubes from the catalyst. We are currently developing the separation techniques.

For the **Figure 8** conceptual diagram, we assume an initial energy input of 1 MWh from the power grid. Depending on the choice of operating point, SOEC can achieve 100% efficiency or even higher (meaning it can utilize external heat). Most commonly, an operating point with 100% SOEC efficiency is chosen, meaning that 1 MWh of energy input will be fully converted into 1 MWh of chemical energy stored in H_2 gas. Thus, 1 MWh of energy leads to the production of 25.4 kg of H_2, based on its higher heating value (HHV) of 39.4 kWh/kg .

In the catalytic CO_2 methanation reaction, 25.4 kg of H_2 reacts with 139.7 kg of CO_2 to produce 50.8 kg of CH_4 assuming 100% chemical conversion rate and selectivity. 12.7 kg of H_2 will get converted into water during the CO_2 methanation process. Even though the CO_2 methanation reaction is exothermic, its initiation requires a high temperature. For the purposes of this diagram, at steady state operation, we assume residual heat recovery while discounting the initial heat input required to reach reaction conditions.

Using Volta Energy technology, CH_4 pyrolyzes, producing carbon nanotubes and H_2. Assuming 100% chemical conversion and selectivity, 50.8 kg of CH_4 yields 38.1 kg of carbon nanotubes (C) and 12.7 kg of H_2 gas. For the pyrolysis pathway an additional 50.8 kg of CH_4 is sourced from the natural gas storage, meaning 101.6 kg of CH_4 will undergo pyrolysis, producing 25.4 kg of H_2 (keeping the energy stored in H_2 constant with the addition of 0.8 MWh equivalent of CH_4 from the natural gas supply).

SOFC electrical efficiency refers to the proportion of the fuel chemical energy that is converted to electrical energy. This efficiency varies depending on the choice of operating point. For SOFC mode, the maximum efficiency at 750 °C using H_2 at 1 atm is 78 %, but this corresponds to essentially zero power output. 60% efficiency corresponds to a voltage of 0.8 V, which is a commonly chosen operating point, which is usually well below peak power but still with enough power to be a practical operating point. Therefore, for our calculation, we take 60% efficiency as the optimal value. With 60% SOFC efficiency, 25.4 kg H_2 will generate 0.6 MWh of electricity. Similarly, for CH_4 gas, with an SOFC efficiency of 60%, 101.6 kg of CH_4 will provide 0.94 MWh of electricity.

Figure 8 | Conceptual Integrated Process of H_2 hubs feature long-term storage and site-specific production

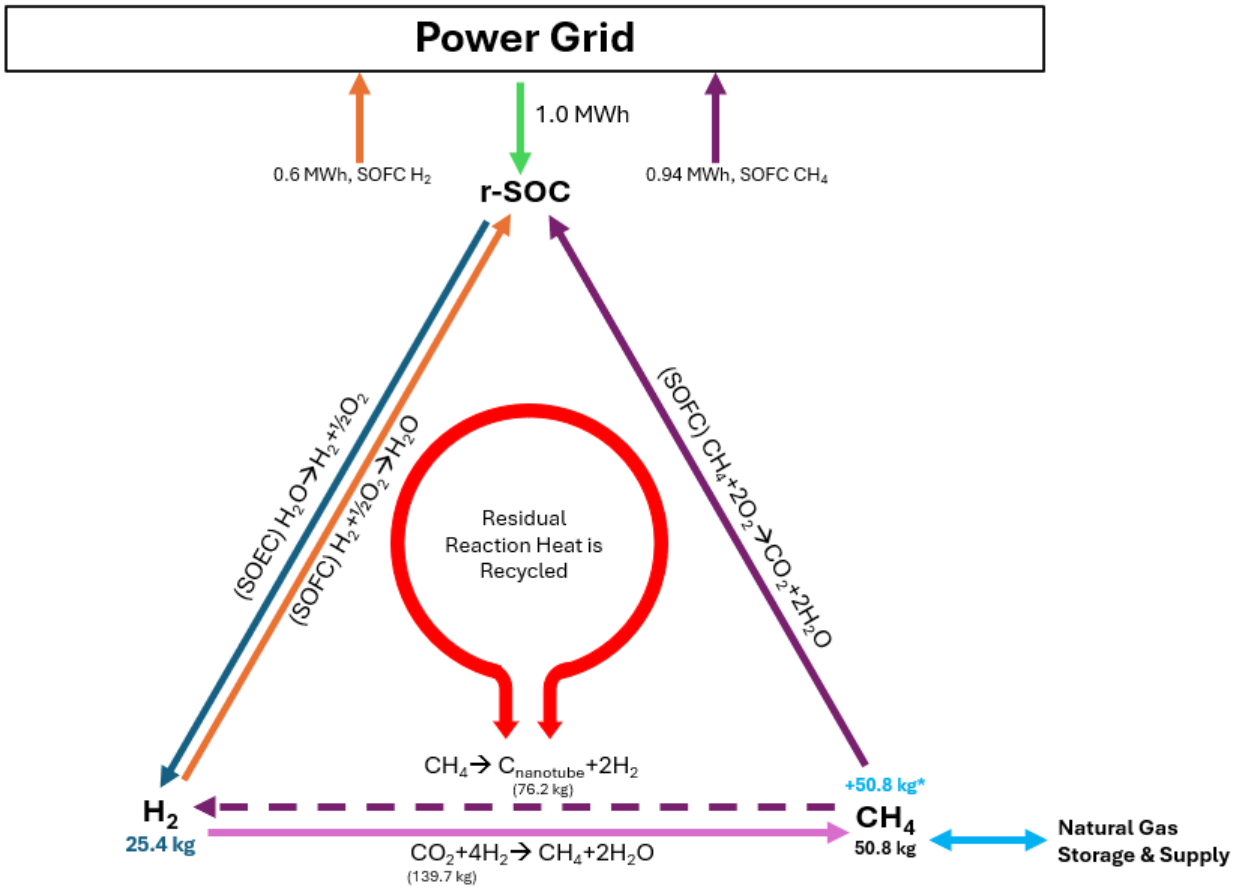

*50.8 kg of CH_4 is assumed to be sourced from natural gas supply, to supplement the 50.8 kg of CH_4 produced through the methanation process.

Dark blue: SOEC H_2. **Orange**: SOFC H_2 (exothermic process). **Red half circle**: Reaction waste heat recycled. **Turquoise**: natural gas storage and supply. **Pink**: methanation reaction. **Dashed-purple**: CH_4 pyrolysis. **Purple**: SOFC CH_4. **Green**: power from the grid.

3.4 Techno-Economic Analysis (TEA)

The economic feasibility of the MSRSOC technology is evaluated using a techno-economic analysis approach. This method involves establishing a levelized cost for producing electricity (LCOE) in Fuel Cell mode and hydrogen (LCOH) in Electrolysis mode. The components of the Techno-economic analysis include estimating the CAPEX for manufacturing and installation of the central MSRSOC system and the accompanying Balance of Plant, and the OPEX which is primarily composed of utility costs. The CAPEX includes the total installation cost of the MSRSOC system which aggregates the process cost model for manufacturing the MSRSOC technology, Balance of Plant and H_2 storage costs. The OPEX includes the price of utilities such as electricity, cost of producing steam (considered as MMBtu equivalent of natural gas), and feedstock involved in the

system operation. This section expands on the technical and financial key aspects considered to establish the scenario specific levelized cost for commodity. Furthermore, the commercialization scope of the technology is explored based on commercial deployment and high-level comparison against competing market available candidate technologies.

Balance of Plant (BOP) model

The BOP model involves the system design and engineering to facilitate MSRSOC stack operation for the identified scenarios. The BOP is based on the Process Flow Diagram developed specifically for our technology and encompasses all unit operations for H_2 generation and compression, power generation, as well as steam generation and heat recovery (ASPEN HYSYS simulations were created for electrolysis and fuel cell mode separately for ease of computing).

The developed simulations for this project are scalable and have the capability of modeling for any Electrical Power input/output (Electrolysis/Fuel Cell), however the economic analysis at ROM level is focused on certain power levels was capped at 200 MW. The calculated CAPEX for the economic analysis is at the Rough Order of Magnitude (ROM) level (±30%).

The operating conditions of rSOC, i.e., temperature, operating voltage (as dominant factors), pressure (less dominant factor, selected close to atmospheric pressure, 126.5 kPa), and the target throughput (in terms of Consumed/Produced electric power for SOEC/SOFC respectively) are the key variables to calculate the mass and energy flow streams, i.e., H&MB, equipment duty and preliminary size and cost analysis for each mode operation.

The next key factor is the rSOC overall efficiency to utilize the waste heat recovery which is the product of thermodynamic (Ideal) efficiency, i.e., ε and voltage efficiency E(OCV). The overall efficiency would determine the excess heat produced during the Fuel Cell mode (exothermic reaction) to preheat the reactants.

Please note that the reversing of electrodes polarity is an over-simplification for simulation development purposes only as the rSOC details are still in development.

Two separate simulations were developed independently for each mode of operation, SOEC as shown in **Figure 9**, and SOFC as shown in **Figure 10**.

Figure 9 | SOEC Simulation Snapshot

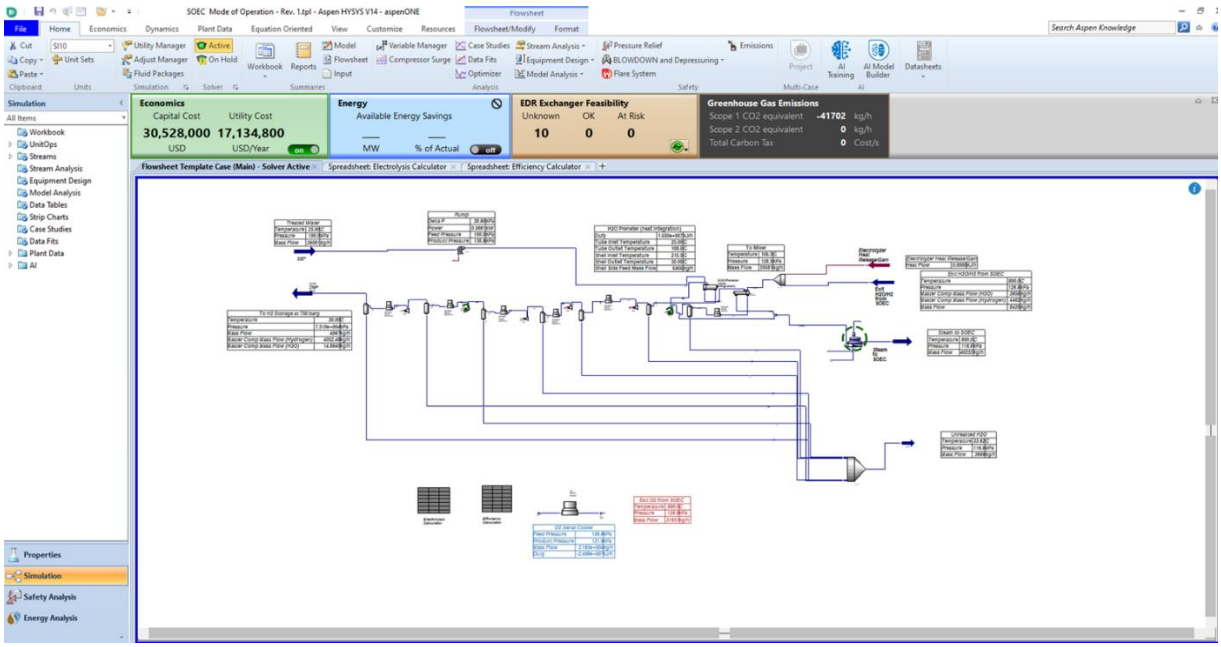

Figure 10 | SOFC Simulation Snapshot

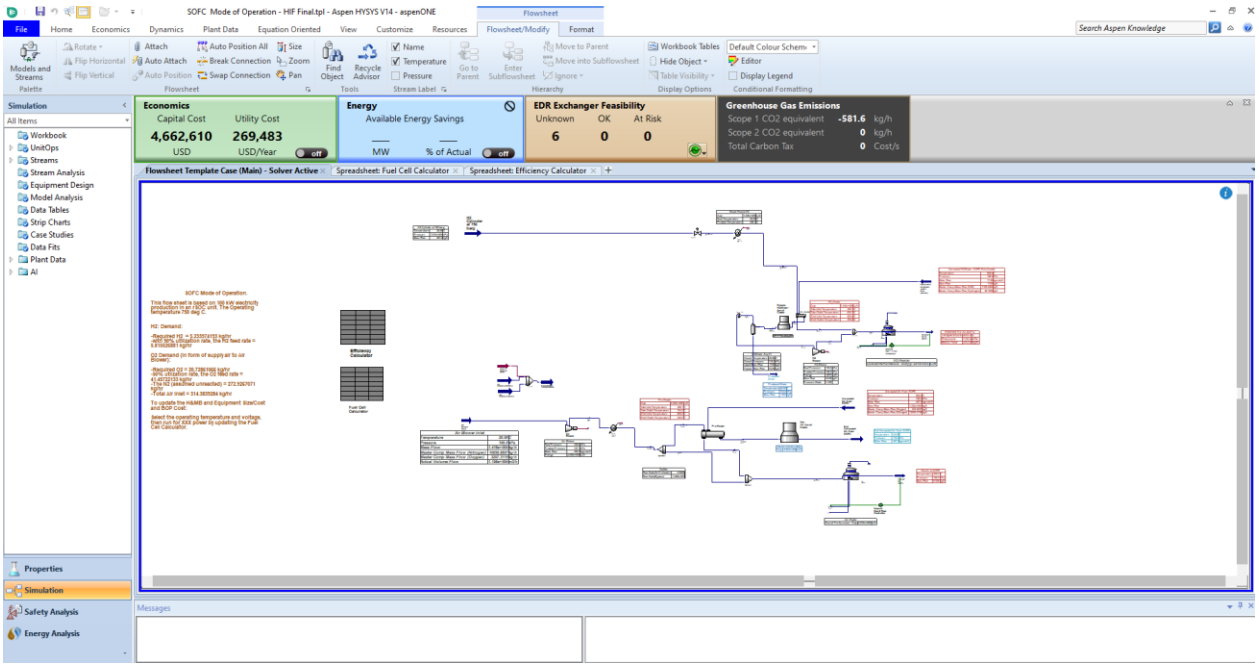

In each mode of operation, the simulation links with two spreadsheet calculators to enter the required inputs for calculating the H&MB as below:

- Efficiency Calculator (exclusive for SOFC)
- Electrolysis Calculator (exclusive for SOEC)
- Fuel Cell Calculator (exclusive to SOFC)

Due to unavailability of sufficient lab data as well as literature references, the focus on calculating the H&MB in the Electrolysis Calculator in the SOEC mode of operation, is only at 800 °C with partial pressures of $H_2O/H_2/O_2$ at 0.9/0.2/0.21 respectively. This enables the simulation to consider operation at thermo-neutral conditions with overall efficiency very close to 1.0 (0.998) with no waste heat recovery requirement or continuous heat input to SOC to maintain its at 800 °C.

The SOCs in both simulations are black boxes in which the material and energy streams are entering into and exiting from it are calculated as specified in above calculators in terms of key factors i.e., operating temperature, applied voltage and electric power input/output.

The efficiency calculator has been developed in each simulation to predict the *ΔG(T)* and the *ΔH(T)* for below reversible reaction:

$$H_2 + \frac{1}{2}O_2 \rightleftarrows H_2O \quad (1)$$

Where:

$$\Delta G(T) = \Delta G_{f(H2O)} - \Delta G_{f(H2)} - 0.5\Delta G_{f(O2)} \quad \text{(J/mol)} \quad (2)$$

$$\Delta H(T) = \Delta H_{f(H2O)} - \Delta H_{f(H2)} - 0.5\Delta H_{f(O2)} \quad \text{(J/mol)} \quad (3)$$

Below family of curves illustrated in **Figure 11** were used to calculate the *ΔH* and *ΔG* at any of operating temperatures 550 °C, 600 °C, 650 °C, 700 °C, 750 °C and 800 °C.

Figure 11 | Thermodynamic Properties of H_2, O_2 and H_2O at different temperatures (K)

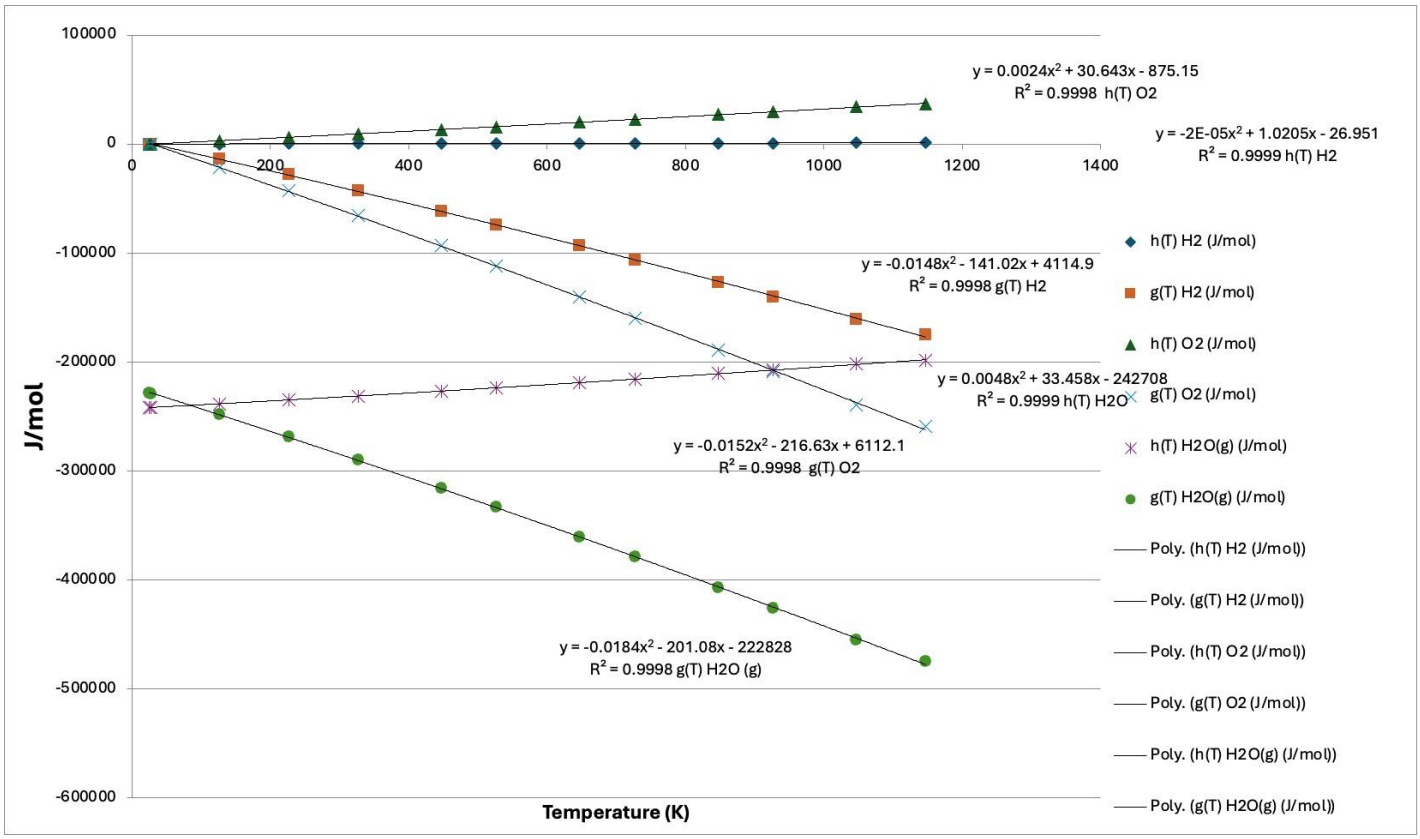

The ideal (Thermodynamic) efficiency is calculated as below in Equations (4),(5),(6),and (7):

Ideal (Thermodynamic) Efficiency

$$\varepsilon = \frac{\Delta G(T)}{\Delta H(T)} \quad (4)$$

$$E0(T) = \frac{-\Delta G(T)}{nF} \quad (5)$$

$$V(th) = \frac{-\Delta H(T)}{nF} \quad (6)$$

$$E(OCV) = E0 - \left(\frac{(RT)}{(n.F)}\right) \ln\left(\frac{pH_2O}{pH_2 * pO_2{}^{0.5}}\right) \quad (7)$$

Where,
R = 8.3145 J.mol^{-1}. K^{-1}

T =Temperature in Kelvin

F: Faraday's Constant, i.e., 96,485 (C/mol e$^-$)

n: number of electrons for oxidation/reduction reactions in terms of mol e$^-$/mol, i.e., 2 for H_2 and 4 for O_2.

The Fuel Cell Calculator utilizes the below inputs for calculating the H&MB and Equipment sizing in each PFD configuration:

- p_{H2O} = 0.03, p_{H2} = 0.97, p_{O2} = 0.21 (i.e., the partial pressures in atm.)
- Operating Voltage: Can be greater than 0.0 and less than 1.1 V (V).
- Operating Temperature: Can be any of 600 °C, 650 °C, 700 °C, 750 °C, 800 °C (T).
- Power Output: 100 kW and above, the minimum economical scale is 1 MW (P).

For each temperature and voltage input a corresponding current density – ID (A cm $^{-2}$) followed by a corresponding power density – PD (W cm $^{-2}$) are calculated with regression analysis through the following family of curves shown in **Figure 12**:

Figure 12 | Voltage (Primary y-axis) vs Current Density & Current Density vs Power Density (Secondary y-axis) Curve

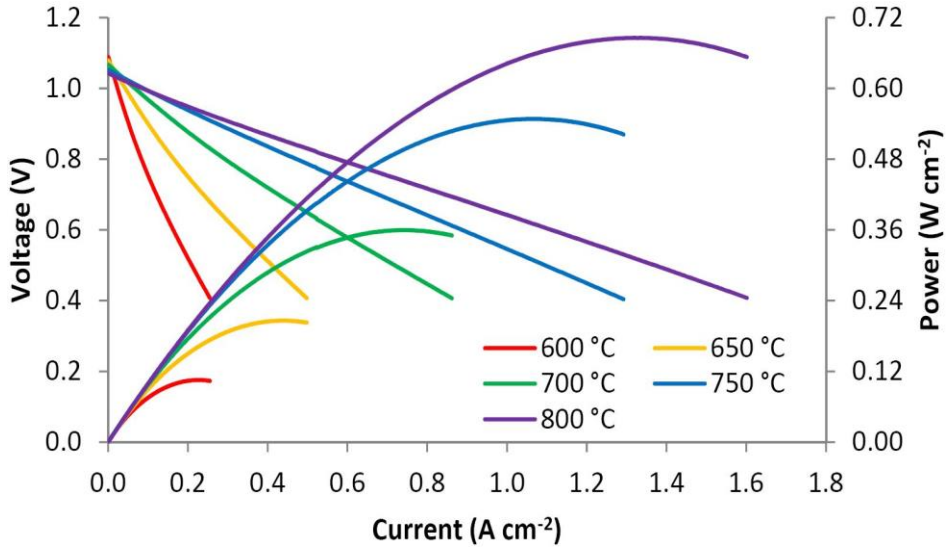

Based on the calculated Power Density PD with the above family of curves and selected power output entry (P in W), the SOC area is calculated, i.e.,

$$A = \frac{P}{PD}\ cm^{-2} \tag{8}$$

The calculated area A and Current Density (ID) will facilitate the calculation of electrical current in the SOFC, i.e.,

$$I = A * ID \text{ in Ampere} \tag{9}$$

With calculating the required I and Faradays' law the required molar flow of H_2 and O_2 are calculated accordingly.

$$r = \frac{I}{nF} \tag{10}$$

Where:

r: reaction rate (mol/sec)

F: Faraday's Constant i.e., 96,485 (C/mol e$^-$)

n: number of electrons for oxidation/reductions mol e$^-$/mol, i.e., 2 for H_2 and 4 for O_2

The utilization rates for H_2 and O_2 are assumed to be 90% and 50% respectively.

Moreover, O_2 is sourced from ambient air (N_2 is considered unreacted in this process) and H_2 is assumed to be produced using the SOEC mode and stored at 450 or 700 barg.

The H_2 feed stream is depressurized in the process with considerations of reverse Joule-Thompson effect from stored pressure (450 barg to 700 barg) to slightly higher than atmospheric pressure. The calculated overall efficiency in the SOFC would determine the waste heat recovery strategy to be used for preheating the de-pressured H_2 all in an enclosure.

Following the first preheat of H_2 feed stream, it will be further preheated with heat exchange of mixture of produced H_2O and unreacted H_2 exit from SOFC at the constant operating temperature. The exit stream of mixture of produced H_2O and unreacted H_2 will be mixed with the second stage of preheated H_2 feed stream to be recycled back to SOFC. Any additional required heat input to H_2 feed stream will be provided with a furnace operated with natural gas if needed. The same furnace with natural gas will be used for unit start up. On the other hand, the air feed stream as the source of O_2 carrier will pass through an air blower to be pressurized slightly higher than atmospheric and then after will be preheated in two stages, first with waste energy out of SOFC same as H_2 feed stream and then with exit mixture of unreacted O_2 and N_2. Any additional required heat input to air feed stream will be provided with a furnace operated with natural gas if needed. The same furnace with natural gas will be used for unit start up.

The overall efficiency in SOFC is calculated as below:

SOC Voltage Efficiency = Operating Voltage/E(OCV)

Where:

Selected Operating Voltage is input to the model.

E(OCV) is calculated as per the Efficiency calculator and the Overall Efficiency = SOC Voltage Efficiency x Thermodynamic Efficiency (using Equation (4)).

The SOFC excess heat generated in the SOC is calculated based on the electrical power output (e.g., 1 MW, 5 MW or 30 MW) multiplied by overall efficiency. The excess heat can be used to preheat the feed streams.

The Electrolyzer Calculator utilizes below inputs for calculating the H&MB and Equipment sizing in each PFD configuration:

- As per literature data, for a typical 500 kW power input at 750 °C or 800 °C, the required total SOC stack area is 1,600,000 cm^2.
- Therefore, for example for a 5 MW power input, the required SOC stack area will be 10 times of 1,600,000 cm^2.
- As per literature data, the current density (I_D) at 800 °C is -0.54885 is A/cm^2 with an operating voltage of 1.008901 V.

Figure 13 | Voltage (Primary y-axis) vs Current Density & Current Density vs Power Density (Secondary y-axis) Curve

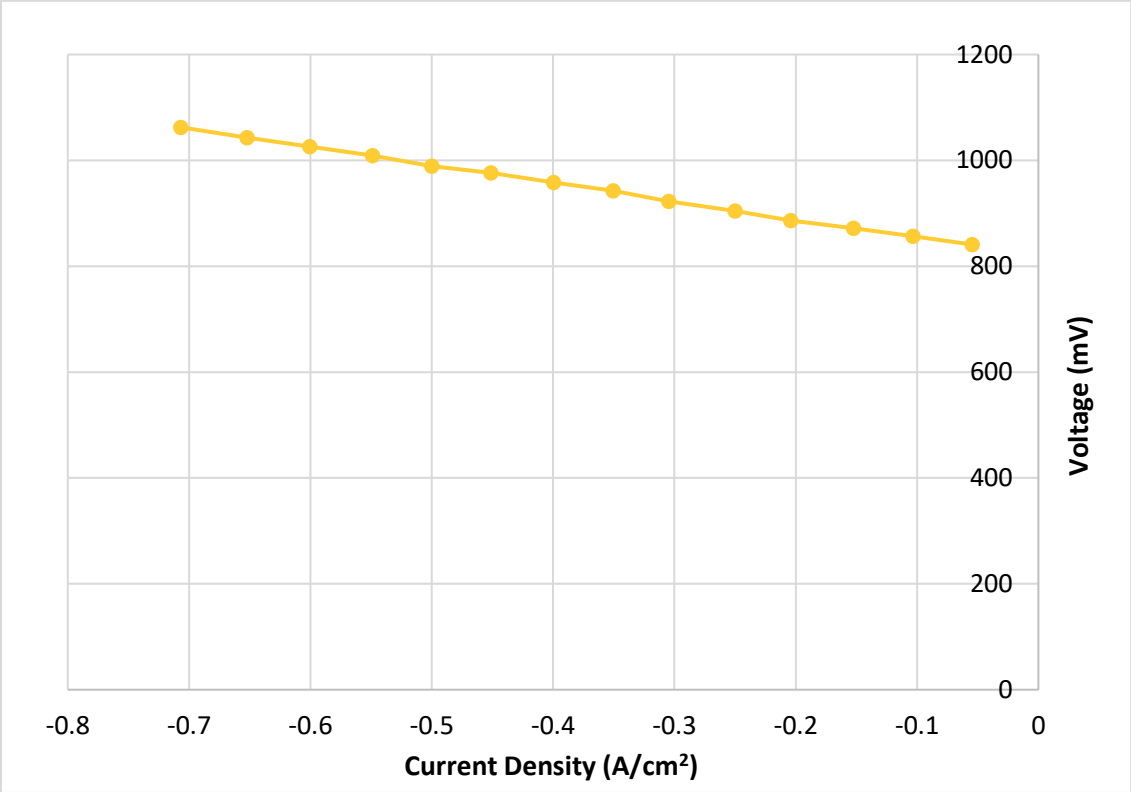

Based on calculated area A for the specified power (i.e., 5 MW, 30 MW and 200 MW) and Current Density (ID) the electrical current in the SOEC will be calculated as (11):

$$I = A * (-\mathrm{ID}) \text{ in Ampere} \qquad (11)$$

With calculating the required I and Faradays' law the required molar flow of H_2O is calculated accordingly as shown in (10).

$$r = \frac{I}{nF} \qquad (10)$$

The utilization rate for H_2O is assumed to be 90% and it is sourced from de-ionized water tank stored at atmospheric pressure. The H_2O feed stream is pumped to 138.9 kPa in this process, it will be preheated with compressed H_2 exit from 1st stage of H_2 compressor in the process. Following the first preheat of H_2O feed stream, it will be further preheated with heat exchange of exit mixture of H_2 and unreacted H_2O from SOEC at constant operating temperature. It should be noted, the waste heat recovery (depending on exothermic/endothermic/thermo-neutral conditions in the SOEC) will be combined with operating temperature of exit mixture of H_2 and unreacted H_2O.

The exit stream of H_2 and unreacted H_2O will be cooled down to separate the H_2O and the H_2 will be compressed in 6 stages with target of maximum temperature exit maintained less than 200 °C. 10% of produced H_2 will be recycled back to SOC mixing with hot water (saturated steam) before entering the furnace. After each stage of compressor, the compressed H_2 will be cooled down to knock out the remaining unreacted H_2O. Any additional required heat input to H_2O feed stream will be provided with a furnace operated with natural gas if needed. The same furnace with natural gas will be used for unit start up. On the other hand, the unreacted O_2 exit stream will pass through an aerial cooler to cool it down at safe at 25 °C temperature before exhausting the atmosphere.

For more details refer to the process flow diagram (PFD) depicted in **Figure 14**.

Figure 14 | Process Flow Diagram (PFD) illustrating BOP for dual mode operation of MSRSOC

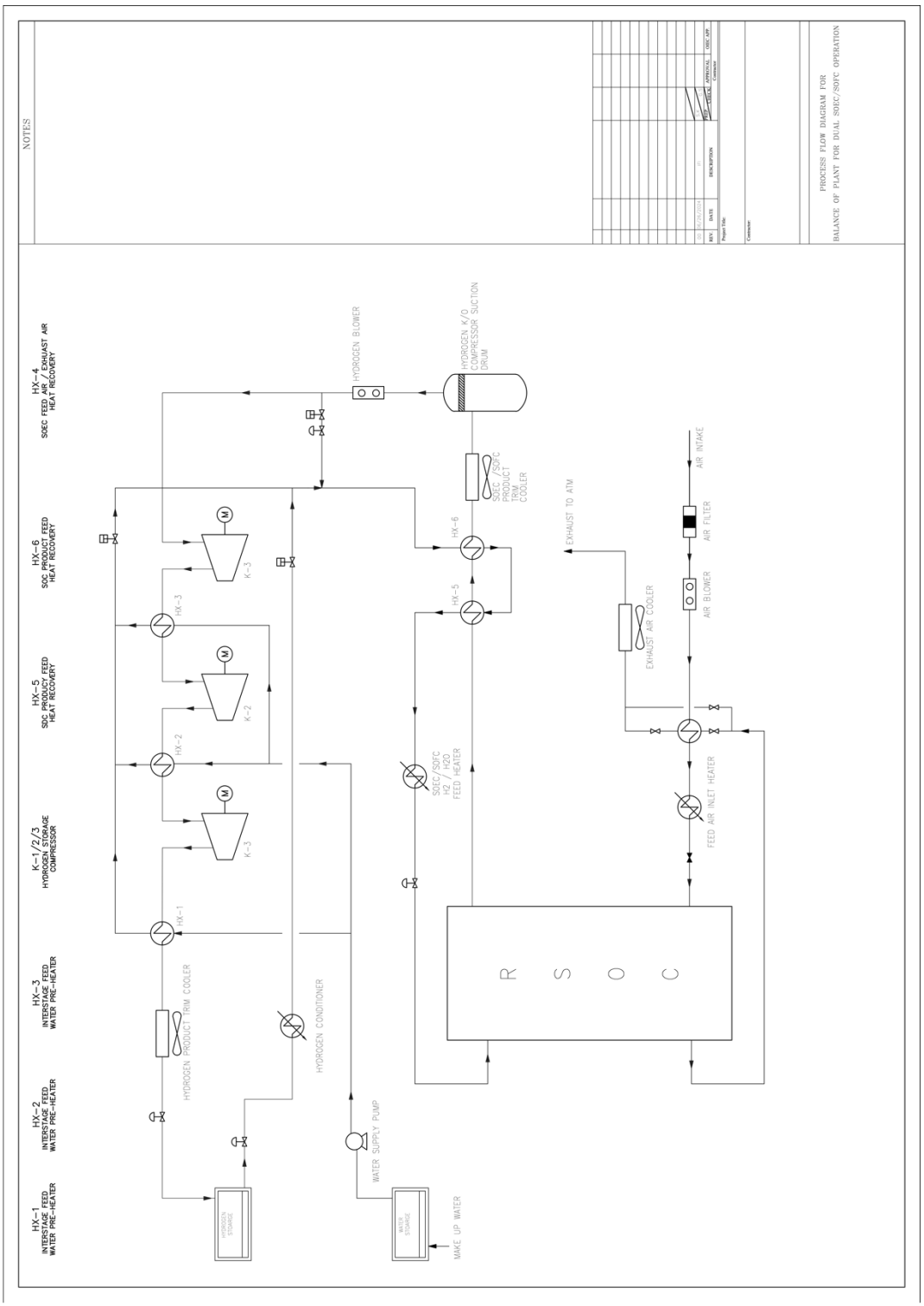

Process Cost Model

The process cost model integrates the direct and indirect costs involved in fabrication and installation of the MSRSOC technology. Based on distinction in the design parameters, the process cost model is influenced by cost of individual cell component materials, cost of interconnects and sealants, fabrication methodology and the associated utility and labour costs. The manufacturing cost of the SOC technology for this project is considered based on publicly available data from NREL to be 212 USD per kW when produced at a nominal economy of scale [17]. SOC technology utilizes industrially available commonplace materials and does not require specific precious metals unlike (proton exchange membrane) PEM based technologies. Furthermore, the MSRSOC developed by FCMML utilizes a stainless-steel metal supported electrode which introduces additional cost savings in comparison with the traditional electrode or electrolyte supported SOCs. This holds the potential for further reductions in the cost of manufacturing the MSRSOC technology when produced on a larger industrial scale in the near future.

Hydrogen Storage

Cost of H_2 storage is sourced from *"Hydrogen Storage Cost Analysis – DOE Hydrogen Program Project"*, information available in the public domain [18].

Utilities and water usage

Steam generation is evaluated as equivalent heat input from natural gas. MSRSOC enables water recovery in fuel cell mode, which enables to offset water demand from electrolysis mode. For our evaluation we assumed demineralized water exported to the facility. It should be noted that the actual cost of water is insignificant in the overall economic analysis.

4. Results and Analysis

4.1 SOC Technology

4.1.1 Electrode Fabrication

SPPS was demonstrated again to produce a fuel electrode. The deposited electrode contained detectable metallic nickel (Ni) and could not idle in dry CH_4 for long periods (1000 hours) at elevated temperatures (750 °C). There was significant carbon deposition, as expected due to the presence of Ni in the nickel (III) tin (Ni_3Sn) catalyst, and the carbon was fully removed via gasification when the electrode was exposed to a CO_2-N_2 atmosphere after the CH_4 exposure process, also as expected. However, the mechanical integrity of the electrode layer was compromised due to the deposition, showing that the material should only be used when current is flowing, or idled in a carbon-free atmosphere such as H_2. Because of a longer than expected closure of the local plasma spray facility due to renovation (> 6 months), a back-up plan of outsourcing the coating fabrication to an industrial vendor was enacted. However, it was later discovered that the composition of the solution that was used by the vendor was not the same as the one that we had previously used, so the analyzed material did not have the expected composition. Future work at the now re-opened local facility will be done to repeat the test and re-evaluate the idling capability. Nevertheless, components other than the electrode can also suffer from carbon deposition under hot idling in dry CH_4, such as steel components of the BOP, so such operation condition should be avoided in any case to prevent material failure in the BOP as well as in the SOC stack.

4.1.2 Metal-Support Fabrication

Tape casting

The challenges of a low-volatility aqueous thick tape casting process to obtain tape with high flatness, uniformity, and oxidation resistance were successfully overcome. Despite the compromise on tape flexibility with low binder and without plasticizer, the final tape can still be cropped into the desired size, which fits the demand of SOC substrate application. Raising solid loading is an effective strategy to prevent slurry particle sedimentation rather than raising the viscosity with an additional binder. This can cause stainless steel sensitization if not effectively removed. The optimized slurry composition is 43 vol% solid loading with -10 μm 430SS powder, with binder and dispersant loadings of 1.7 wt.% and 0.47 wt.% of the steel powder weight, respectively.

Substrate sintering

By applying dense sintering with fine particles to preserve only porosity from the pore former particles, a microstructure with uniform porosity was created that can help to prevent breakaway oxidation by minimizing the surface area. PMMA, as the pore former, burns out to a sufficient extent at 350 °C without causing sensitization. 29 vol% porosity could be obtained by adding 55 vol% PMMA and sintering at 1200 °C for 4 hours. Sintering steel tape in a high flow rate of high-purity H_2

for an extended time can be used to remove carbon and reverse sensitization if the carbon removal was insufficient during previous outgassing and pre-sintering steps. The carbon removal rate for temperature, H_2 pressure, and flow rate needs further investigation.

Magnetic field generation

This work demonstrated the fixture designs required to create aligned porosity by both freeze casting and slip casting, with the option to apply an additional uniform magnetic field. The actual measured value from a handheld Tesla meter agrees with the theoretically predicted magnetic flux density design value. In addition, process parameters of magnetic slip casting, including steel particle size, pore former size, pore former volume fraction, solid loading, and the time for slurry to stay under a magnetic field, were optimized to create multiple crack-free substrates. The freeze-dried samples' sintering time is one hour at 1200 °C, while the slip-cast sample would require two hours of sintering at the same temperature.

Random porosity substrates

The effect of various spherical PMMA pore former sizes and volume fractions on gas permeability, surface roughness, pit width and depth, and steel surface-to-volume ratio has far-reaching implications. With its balanced performance, the PF60 at 0.45 volume fraction holds promise as a metal support for plasma-sprayed solid oxide cells. Moreover, our findings could be useful for applications such as support structures for oxygen separation membranes, catalyst supports, and metal water filters, improving gas permeability and reducing surface-to-volume ratio. This research also paves the way for developing a scalable tape-casting method, potentially inspiring future advancements in the field.

Densely sintered porous 430 stainless steel produced by powder metallurgy has sufficient mechanical strength as a metal support for SOC application. The material shows very ductile behaviour. The yield strength, often lower than the flexural strength, as compared to the requirement for PEMFC bipolar plates, greater than 59 MPa for vehicle application. All tested specimens, ranging in porosity from nearly 0 to 46.5%, met this requirement. There was a significant drop in yield strength with rising porosity from 380 MPa to 120 MPa over a porosity range of nearly 0 to 46.5%. EBSD mapping suggests that the linear shear motion applied to the slurry did not create any preferred material orientation. Misorientation mapping suggested that the throats created by the porosity had the most misorientation during three-point bending loading, which implies that those regions experience the highest degree of deformation.

Aligned porosity substrates

The study also compared different fabrication methods, including freeze casting and magnetic slip casting, highlighting the advantages of magnetic field alignment in producing substrates with better mechanical properties and more consistent porosity. These findings underscore the importance of considering porosity distribution and alignment in designing and fabricating materials for applications requiring specific mechanical properties. Among the aligned porosity samples, the metal supported cells (MSC) samples demonstrated relatively strong mechanical properties compared to freeze-dried samples, while the gas permeability and other structural properties were close to that of FC. If the oxidation problem can be resolved, the more convenient fabrication makes it a more promising method to create an aligned porosity substrate.

The study of aligned porosity substrates under three-point bending testing revealed several critical insights. Samples with a gradient in porosity demonstrated a significant difference in mechanical performance depending on their orientation during testing. Specifically, when the less porous side faced up, it exhibited greater strength than when it faced down. The elastic modulus was found to be more sensitive to alignment of the porosity than yield strength, with the reduction in effective load-bearing area due to porosity having a larger impact on the material's stiffness. Aligned porosity substrates, produced using magnetic field alignment of pore formers, showed enhanced stiffness, strength, and toughness due to improved structural integrity and load distribution.

4.2 Smart-Hydrogen Hub (SH2) Development

The development of suitable models and associated controls as well as the detailed system-level simulation of reversible SOCs, supports the practical value of SOCs for integration with the power grid for energy buffering and other future applications. Our findings indicate that rapid response with controlled SOCs in either FC or EC modes is achievable, with response times on the order of fractions of a second for meeting power requirements expressed as dispatch signals from the IESO.

In the system-level analysis of response times, it is assumed that a 5 MW system would likely be designed as ten 500 kW stacks of cells, each of which can be operated independently. In this way, the number of stacks to be put into service can be adjusted according to the demand at a given time. At least one stack would be in "hot stand-by" mode when it is expected to be required to generate electricity or H_2 within a relatively short time period. The operating temperature is achieved by using either a starter burner or Joule heating to raise the temperature to the operating range, after which the by-product heat from the system is sufficient to maintain its temperature. As one stack approaches the pre-defined load level at which a second stack will soon be required, the second stack is put into hot stand-by mode so that it will be ready to respond rapidly to a control signal once the additional power is required (in fuel cell mode) or ready to be used (in electrolysis mode). Additional stacks will be called into service as electricity demand/supply increases (SOFC/SOEC mode).

For changing between the two operational modes, electrical response time to a control signal can be quite rapid, and the fuel cell can change its direction of electrical current flow nearly instantaneously compared to the time that is required to change the flow of reactants to the system from the fuel being used in electricity production mode to the steam being used in electrolysis mode or vice versa. The time that it takes to achieve a change-over between modes depends on the size of the system and flow rate of the reactants, which together determine how long it takes to flush one set of reactants from the system and replace them with the reactants for the other operational mode. To avoid unintended oxidation of the fuel electrode catalyst when changing over from fuel reactant in fuel cell mode to steam reactant in electrolysis mode, a two-stage reactant changeover is likely to be chosen, wherein the system is first flushed from fuel-only to a 50-50% mixture of fuel and steam, and then sufficient time is allowed for complete flushing of the system prior to starting the demand for electrolysis. The system can then be switched over to a 90% steam/10% fuel mixture once the electrolysis process has begun, thus avoiding an unintended situation where steam is being delivered to the system while it is still in fuel cell mode. That situation could lead to unintended oxidation of the fuel side catalyst material due to the combination of demand for current and the absence of fuel from which to produce the current, so that the fuel-side catalyst would effectively be used by the

system as fuel, being oxidized instead of H_2 or CH_4. Although the oxidation of the fuel catalyst is chemically reversible once H_2 is re-introduced to the fuel-side chamber, the mechanical stress from the constrained volume expansion can be sufficient to crack the electrolyte, and is therefore best avoided.

4.2.1 Electro-chemical Process Modelling

An important first step in developing our system-level simulations is to ensure that our SOC models at the fundamental level of cell operation, are verified. We performed model verification in a couple of ways: 1) in steady state, comparing the FEA model in COMSOL multi-physics simulation and the SOFC model running in Matlab/Simulink/Simscape, and 2) in a dynamic setting, co-simulating the FEA model within Simulink, and comparing these results against our derived lumped-parameter nonlinear state-space model in SOEC mode, running in Simulink. These simulations were extremely computationally intensive and required considerable time. Although these validation studies resulted in positive outcomes, we would have preferred to perform further verifications, across a broader range of system parameters, but time constraints limited our studies. The results of our model derivations, as well as subsequent verifications, are provided in Appendix 2.

4.2.2 Controller Design

Controller design was somewhat complicated by the nonlinear nature of the SOC system, as well as controllability issues owing to the mathematical structure of the SOC system. Contending with nonlinearity led to a gain-scheduling approach, as described above, which presented challenges in terms of solving a complex series of algebraic equations to determine system operating points. However, we have systematized the solving of these equations so that they can be performed rapidly on a computer (virtually instantaneously), allowing system parameters to be tuned during system operation as well as within a fraction of a second following an IESO dispatch signal. The controllability issues we faced for the various linear systems corresponding to the operating points were, fortunately, not too problematic since any immovable system eigenvalues had (relatively large) negative real parts, allowing us to proceed with controller design on the controllable/observable (minimal) realization.

Closed-loop simulations (SOC with controller) produced favourable results for both SOFC and SOEC operations. We have produced simulations incorporating IESO provided guidelines for following dispatch signals for electrolysis mode power consumption supplemented by our own interpretation of the same for power generation. Please see Appendix 2 for detailed results. In the case of SOFC integration into the power grid, we have attempted to provide added realism, by incorporating a small power grid model (with simulated excitation-controlled generator) to give a sense of the SOC's ability to buffer additional loading on the grid from turbine-based electricity production. The simulations indicate that SOCs are especially suited to power grid buffering, owing to their rapid response capability, partly enabled using suitable controls. The coupling of SOFCs with gas turbines may be particularly synergistic not only due to ability of SOCs to buffer changing power needs while spinning turbines with rotational inertia require more time to change their operating condition. The two power generators can also combine to generate electricity at a higher efficiency than either technology can achieve alone, do the fact that SOFCs can operate at higher electrical efficiency when they have a high concentration of fuel. Thus, allowing some fuel to escape the SOFC unreacted keeps the concentration high in the SOFC at all times, allowing it to produce more power, while the

unreacted fuel can then power the gas turbine. Together, such systems have been reported by Siemens Westinghouse to generate power at 70% electrical efficiency, higher than gas turbines can achieve alone or even in combined cycles, and at higher power outputs that SOFCs can achieve when they operate at such a high efficiency on their own.

4.3 Storage and Decarbonization

As detailed in Appendix 3, because of the unique characteristics of H_2 molecules, being diatomic structure with the lightest and smallest atoms, H_2 gas has extremely low boiling point (- 252.9 ^oC), low density, volume energy density, and high diffusivity. Any attempt to liquefy H_2 gas is a process of energy intensive and thus with low net energy efficiency, furthermore, H_2 gas can diffuse through metals, resulting in "hydrogen embrittlement".

Therefore, even though H_2 is a promising source of green energy, it presents challenges in its storage and transportation. Cylinder/tanks storage is suitable for short-distance and small-quantity use of H_2; blending H_2 gas with natural gas serves as a practical method for short-term H_2 storage and transportation. For long-term storage and transportation, a practical way is to convert H_2 into carrier fuels, such as CH_4 and methanol for industrial use. Our calculations have confirmed that transforming H_2 into CH_4 and methanol has energy conversion efficiencies of 81%, and 84%, respectively, with the added benefit of utilizing captured CO_2.

Converting H_2 gas to carrier fuels not only serves as a long-term H_2 storage but also a decarbonization pathway, because the processes of the conversion utilizing the captured CO_2. The following **Figure 15** highlights the decarbonization pathways.

Figure 15 | Pathways for Green H_2 Production and CO2 Utilization/Decarbonization Facilitated by Reversible SOC

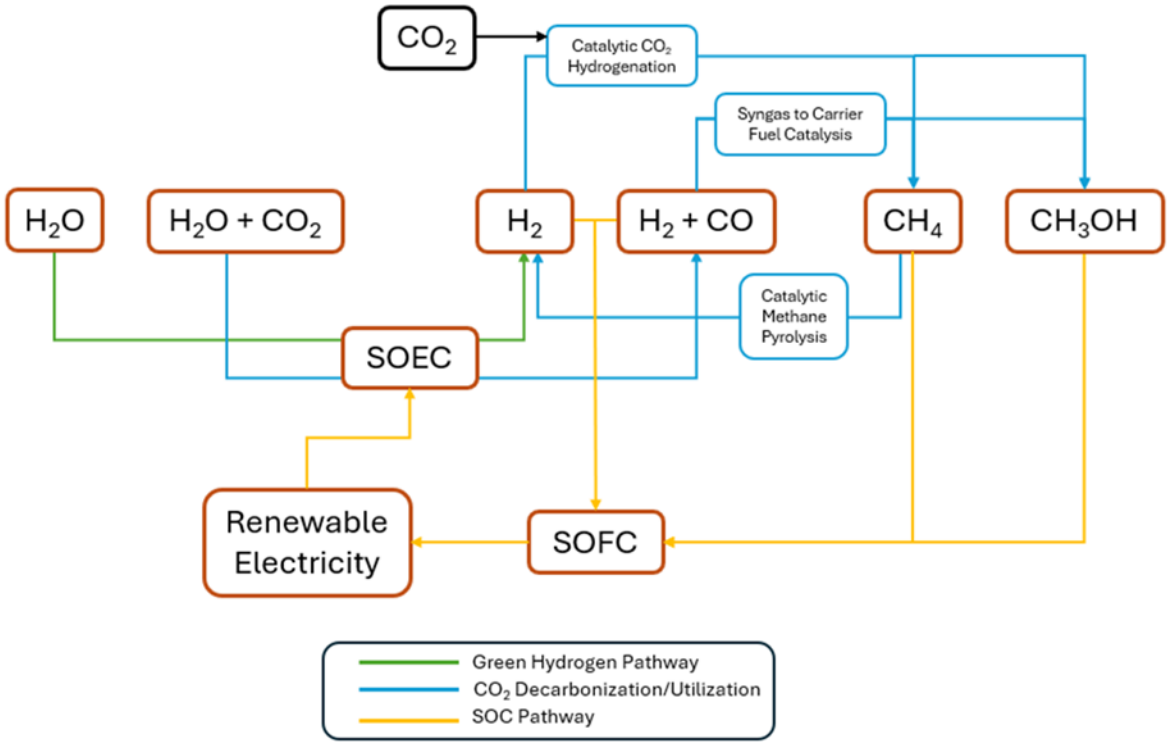

Both the processes of converting H_2 gas along with captured CO_2 to CH_4 and methanol are decarbonization pathways. Our calculations indicate that 1.37 tonne of captured CO_2 is utilized for every tonne of methanol is produced through either direct CO_2 hydrogenation or syngas pathway, and 2.74 tonne of captured CO_2 is utilized for every tonne of CH_4 produced. In addition, CH_4 pyrolysis also serves as a unique decarbonization pathway, as it indirectly converts CO_2 into solid high value carbon material, a negative CO_2 emission pathway. Our study demonstrates that CH_4 pyrolysis can occur even at 500 °C when using the catalyst developed by Volta Energy, producing twice the stoichiometric and one time the stoichiometric amount of H_2 gas and carbon nanomaterial, respectively, from CH_4.

Although we have not yet completed a levelized cost estimate for H_2 production using the CH_4 pyrolysis process, compared to conventional catalytic pyrolysis, our process is qualitatively more sustainable as our catalyst is cost-effective and operates at lower temperature. In comparison to non-catalytic pyrolysis, which typically occurs at temperatures above 1100 °C, our process has the following two advantages: 1) a much lower reaction temperature of 500 °C, 2) the production of carbon nanotubes instead of carbon black.

Volta Energy's developed catalyst is cost-effective and sustainable, as it does not rely on any noble or expensive metals or materials, and can be easily produced at scale. As with any chemical process, the production of Volta Energy's catalyst will have a carbon footprint. However, the primary H_2 production pathway, SMR (steam methane reforming), also relies on catalysts. Volta Energy's catalyst facilitates pyrolysis at 500 °C, a temperature significantly lower than those required for SMR. Therefore, from these perspectives, the production of the catalyst will not increase the carbon

footprint of the H_2 generated. Compared to CH_4 pyrolysis without catalyst, the Volta Energy process may also not increase carbon footprint, as it operates at 500 °C, significantly lower than the 1100 °C required for non-catalytic pyrolysis. For example, based on our simplified calculations using HYSYS, heating 1 ton of CH_4 at a flow rate of 1 mol/h to 500 °C instead of 1100 °C would save 2.8 GJ energy. Even more energy is saved when accounting for the energy required to maintain 500 °C rather than 1100 °C throughout the reaction time.

All the processes—methanation, methanol production, and CH_4 pyrolysis—require effective catalysts for efficient transformation. Volta Energy has designed and synthesized catalysts for these processes, and thorough characterization and initial reaction tests have shown them to be promising for the intended reactions. For example, the catalysts for methanol production can prevent the catalyst from sintering, thus sustaining catalyst's activity for an extended reaction period; CH_4 pyrolysis facilitated by Volta Energy's catalyst occurs at 500 °C, producing carbon nanotubes that have been verified with SEM and XPS analyses. CO_2 direct hydrogenation to methanol and CH_4 pyrolysis will be further pursued due to their promising potential, as developed by Volta Energy.

4.4 Techno Economic Analysis

The results for this section are presented in Section 5.

5. Economics of Proposed Technology

5.1 Fuel Cell Supply Curves – Levelized Cost of Electricity (LCOE)

Fuel cell supply curves using H_2 as fuel were produced starting from the data shown in **Figure 12**, showing MS-SOC performance when operating on H_2 over a range of temperatures. A target operating temperature is 750 °C, chosen for a balance of good performance and longevity. Fuel cell supply curves were generated for 750 °C and for 800 °C, the latter providing better performance but potentially at a trade-off of faster performance loss over long operating times, contributing to shorter lifespan. At temperatures below 750 °C the power output is lower and therefore a larger system capacity would be required raising the capital costs. For the purpose of this study that was deemed to be impractical because the cell degradation rate at 750 °C is sufficiently low that a good operating lifespan is expected.

As shown in **Figure 12**, the power output and voltage of a fuel cell vary widely with current density, leading to a wide choice of operating points that in turn affect the operating efficiency and initial design of the power plant. A standard power plant size of 5 MW was chosen for the analysis, considering a stationary generation unit large enough to contribute to the power grid. The target operating point was chosen as 0.8 V per cell, to provide a balance between high operating efficiency (60% electrical efficiency on an HHV basis) and size of the system (sufficient power output to avoid the need for excessive system size and cost). At a higher voltage, the operating efficiency would be even higher, but the power output for each fuel cell would be lower, so more cells would be needed for a given system output. Alternatively, a higher power density could be chosen that would allow for a smaller system size but would then require more fuel to operate. In choosing the system size as nominally 5 MW when the voltage is 0.8 V, the actual power output of the system can be higher than the power output at the targeted operating range, reaching more than double the power output but at a trade-off of requiring more fuel for a specified quantity of electricity.

When using H_2 as the fuel, the cost of the H_2 and its source (green vs. grey, for example) can vary widely, and thus both the cost and environmental profile of the electricity production would vary accordingly. The impact of both H_2 cost and operating condition for an SOFC operating on 750 °C on H_2 are shown in **Figure 16**. The H_2 cost has a direct and linear impact on the electricity cost. The choice of operating condition has a more variable effect. At power densities leading to output powers below the nominal 5 MW target operating range, the choice of power output does not have as strong an impact on the cost of electricity as the H_2 price. In operating at power densities beyond the target range, the influence of output power becomes stronger as the system is pushed farther and farther beyond its target operating range. When the power output approaches twice the nominal level, the cost of electricity more than doubles as the operation becomes less and less efficient. Therefore, it is advisable to size the system so that the expected typical power output levels fall near the middle of the range that the system can produce.

Figure 16 | Fuel cost of electricity for a 5 MW nominal SOFC system operating on H_2 fuel at 750 °C for a range of power outputs.

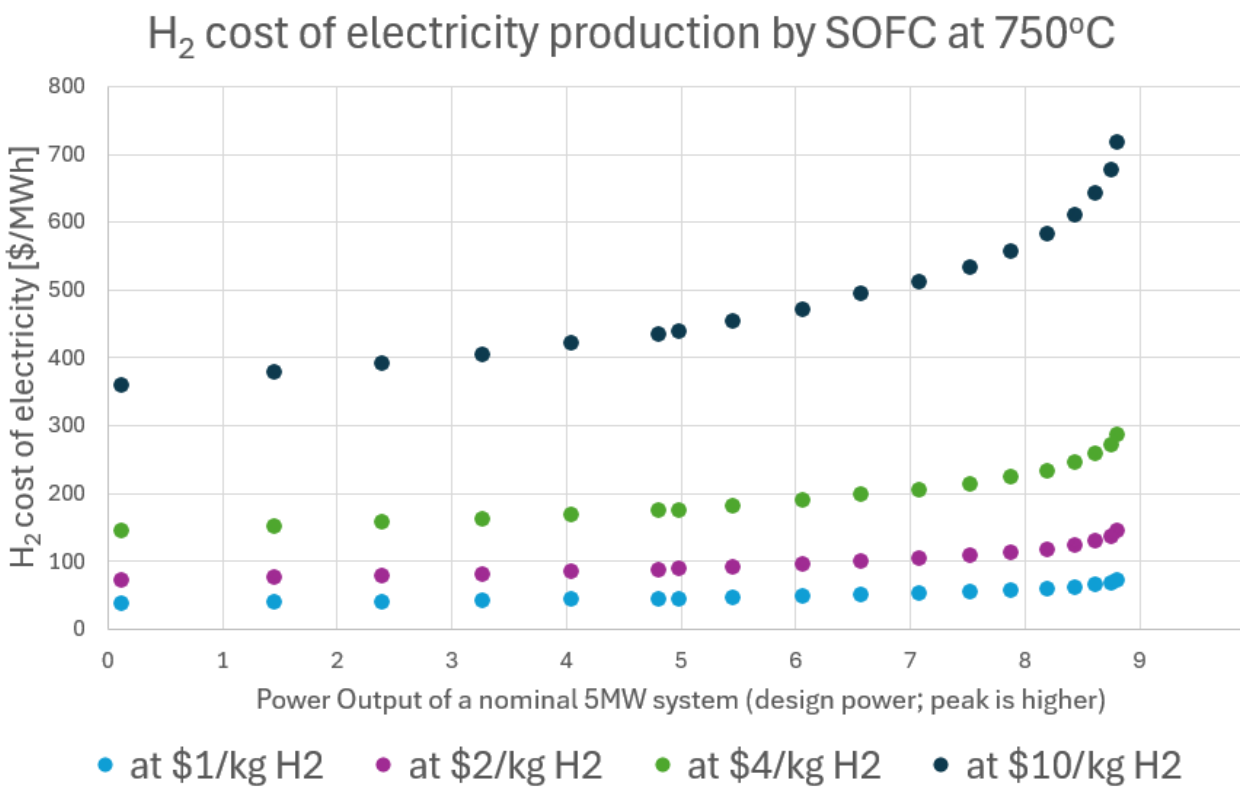

The costs shown in **Figure 16** are the fuel costs of producing electricity, showing how changing the operating condition for a given system alters the efficiency, and therefore the fuel cost. Since the portion of fuel enthalpy that does not contribute to the electrical energy is instead converted to heat, the fuel cost of electricity production inherently includes the cost of maintaining the high temperature of operation of the system, provided that adequate insulation is included in the balance of plant design, which is typically true and within the control of the system designer. The only additional cost related to the high temperature of operation is the start-up cost, which is not included in the steady-state calculation reported here. The start-up process can be performed with either a starter burner, which burns a small amount of the fuel to raise the system temperature to the operating range, after which the burner is turned off and the fuel re-directed exclusively to the fuel cell system. Alternatively, Joule heating could be used by incorporating wires into the stack design that would be used to start-up the stack via resistive heating, after which the current to those wires would be turned off once the stack reaches operating temperature range. Once operational, the stack's by-product heat maintains its temperature. Since the start-up portion of the operating cycle is a very small fraction of the operating time, the amount of either fuel or electricity used in starting the system would not be sufficient to contribute greatly to the fuel cost of the electricity produced. However, the cost of a starter burner was included in the system cost calculation, since the hardware is required to be included in the balance of plant. Since the operating efficiency of electricity production is approximately 50% higher for SOFCs than for PEMFCs, the fuel cost of electricity production from H_2 via PEMFCs would be approximately 50% higher than that produced by SOFCs.

In addition to the fuel cost, the system size greatly influences the levelized cost of electricity (LCOE) via the contribution of both the fuel cell stack cost and the balance of plant (BOP) cost, which together

form the capital expenditures (CAPEX) required to produce the electricity. The fuel cost was considered as the primary operating expense (OPEX), which was combined with the CAPEX to calculate an estimated LCOE when using H_2 at 750 °C. The OPEX would also include maintenance operations required to keep the system operational. As a new technology, there is no historical data to draw from in estimating the maintenance costs. However, it is worth noting that since the stack itself has no moving parts, maintenance would be minimal. On the other hand, performance degradation due to chemical processes such as oxidation of components or material processes such as microstructural coarsening of the electrodes would likely limit the lifetime of the fuel cell stack, in the early stages of deployment of the technology. Since these mechanisms are not fully reversible, maintenance time would not be the main mode of intervention to deal with the consequences of performance loss over time. Instead, the lifetime of the stack was estimated to be only 5 years for early generations of the technology, so that the hardware cost of the stack would be incurred every 5 years of operation by replacing the stack component of the system.

The BOP, on the other hand, consists of more mature technology for compression of the fuel in electrolysis mode and for controlling and regulating the electrical output and flow of gases in both fuel cell and electrolysis modes. A 10-year lifetime was assumed for the BOP in the LCOE calculation as a conservative choice, although historical data suggests that BOP lifetimes may be indeed much longer than 10 years. Such a potentially unrealistically conservative estimate for BOP life was chosen in part to offset the uncertainty in the stack lifetime estimation based on extrapolation of much shorter durability tests in the absence of longer-term historical data based on implementation of the new MS-SOC technology.

Figure 17 shows the levelized cost of electricity in $/MWh for a nominally 5 MW SOFC system operating in H_2 at 750 °C, for a range of operating conditions analogous to those shown in **Figure 16**. Those conditions influence the power density and efficiency of the fuel cell output, contributing to the CAPEX and OPEX, respectively, as a result.

Figure 17 | LCOE for a 5 MW (nominal) SOFC system operating on H_2 at 750 °C

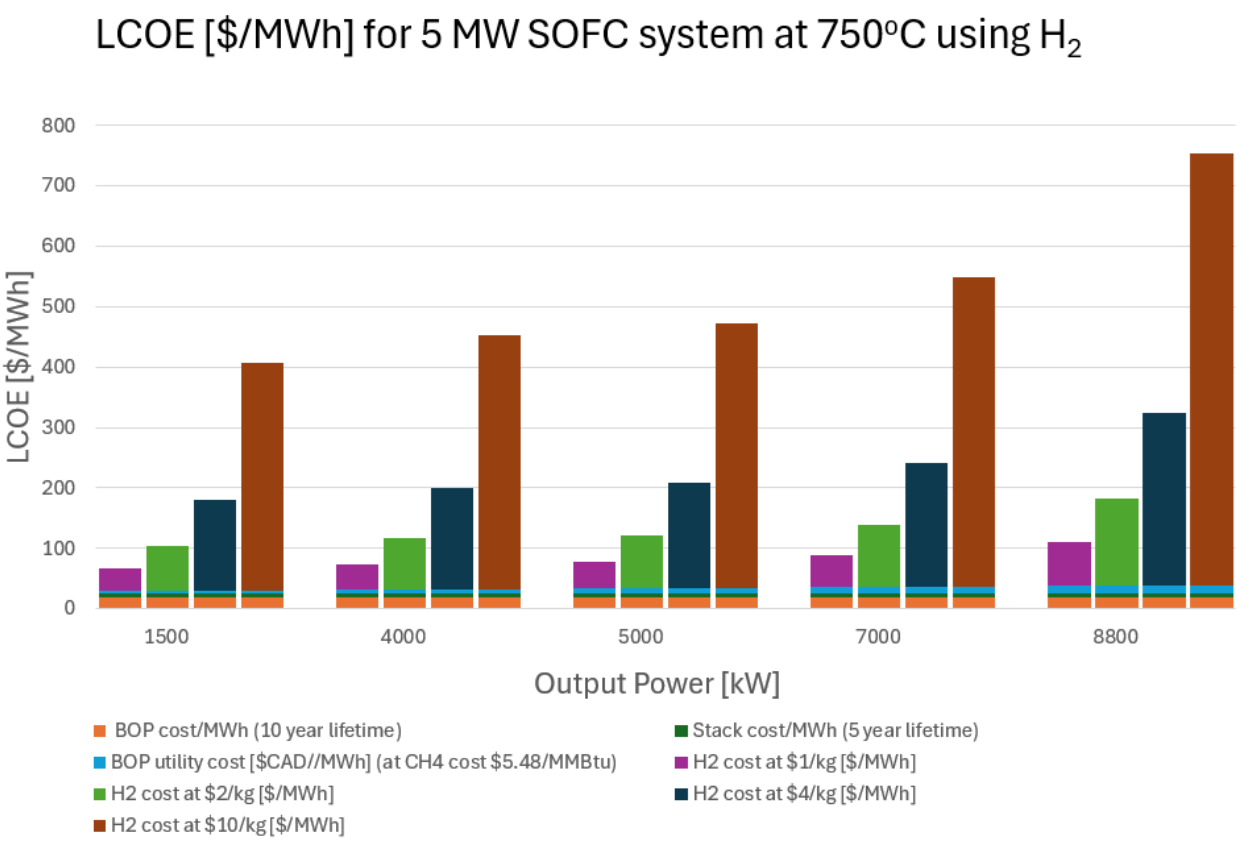

As shown in **Figure 17**, the LCOE depends very strongly on the fuel cost. At the target operating condition of 5 MW, the LCOE ranges from \$80-480/MWh, as the H_2 cost ranges from \$1-10/kg H_2. Even at the lowest cost of H_2 considered, the stack cost and BOP cost together contribute less than half of the cost of electricity compared to the cost of H_2. Even so, building a larger system that distributes the BOP cost over a larger quantity of electricity production has the potential to decrease the LCOE by up to \$40/MWh. On the other hand, using lower-cost H_2, potentially produced from curtailed or surplus power, would have an even larger impact on reducing the cost of electricity production by fuel cells using H_2.

Similar fuel cell offer curves were produced for operation at 800 °C, using the data in **Figure 12** for the fuel cell performance. At this operating condition, higher efficiency and power output can be achieved, but potentially at the expense of a shorter lifetime. Since historical lifetime data are not available for the MS-SOC technology, the same 5-year stack lifetime and 10-year BOP lifetime were considered for the LCOE calculation, to show the impact of adjusting the operating temperature.

Figure 18 shows the fuel cost of electricity production by an MS-SOC operating on H_2 at 800 °C. Since the same operating voltage is chosen as a target operating condition, the higher performance of the fuel cells at 800 °C does not influence the fuel cost. The fuel cost is determined only by the efficiency, which is determined by the operating voltage. As mentioned previously, this fuel cost inherently includes the cost of maintaining the system temperature, while the cost of reaching the system temperature at startup is minimal compared to the steady state fuel cost. On the other hand, the size of the system required to produce the given electrical demand has some impact on the cost, particularly at higher output power levels, as seen in **Figure 19**.

Figure 18 | Fuel cost of electricity production for an MS-SOC stack operating at 800 °C on H_2

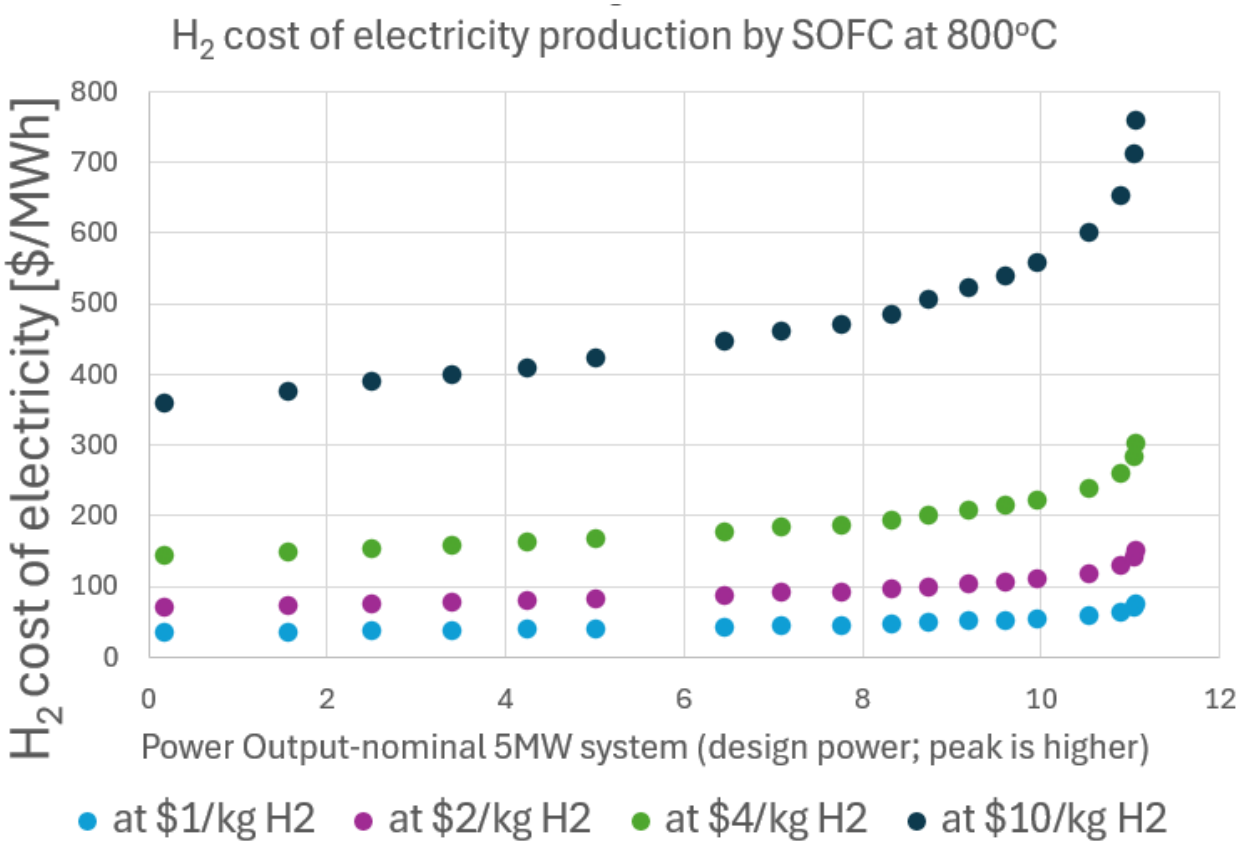

Figure 19 | LCOE for an MS-SOC system operating on H_2 at 800 °C

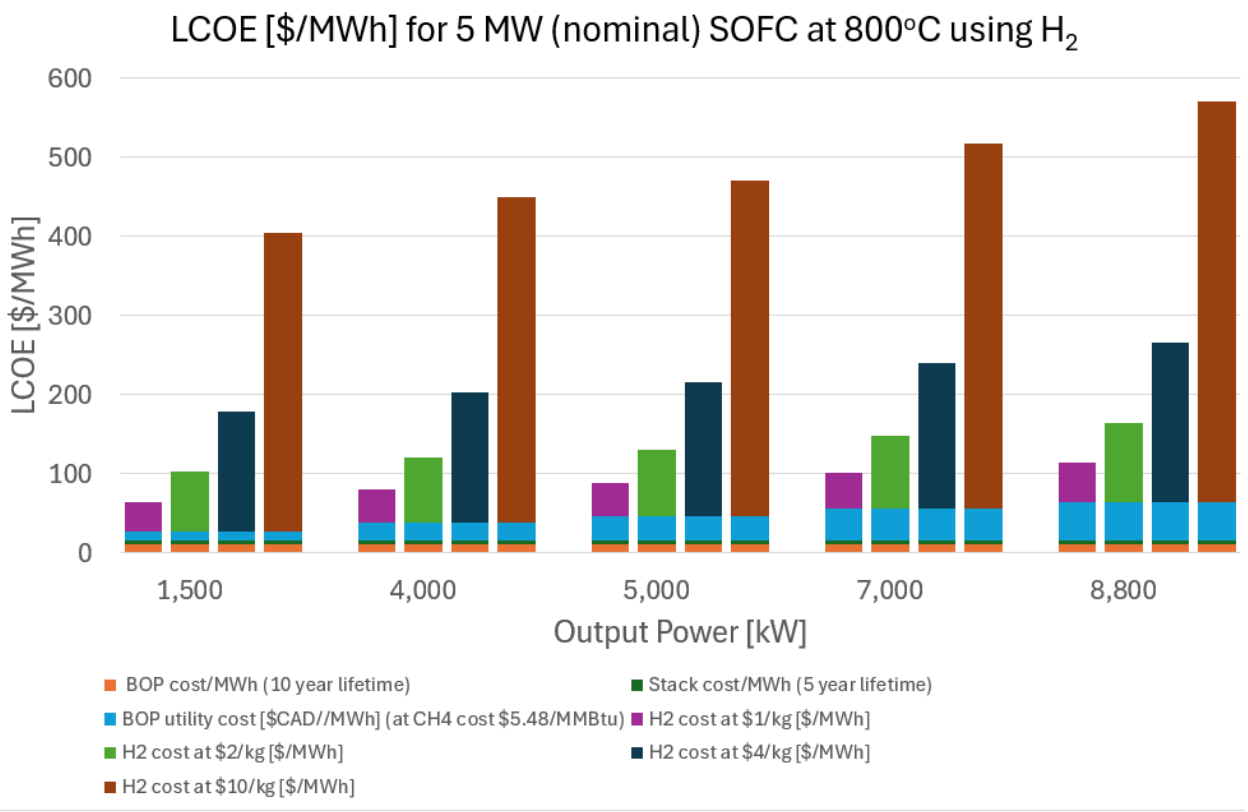

For both operating temperatures considered, the fuel cost of electricity production dominates the LCOE when operating on H_2 (as mentioned previously, these include the cost of maintaining the stack temperature).

Figure 20 | Performance data of MS-SOCs operating on both H_2 and CH_4 at 750 °C

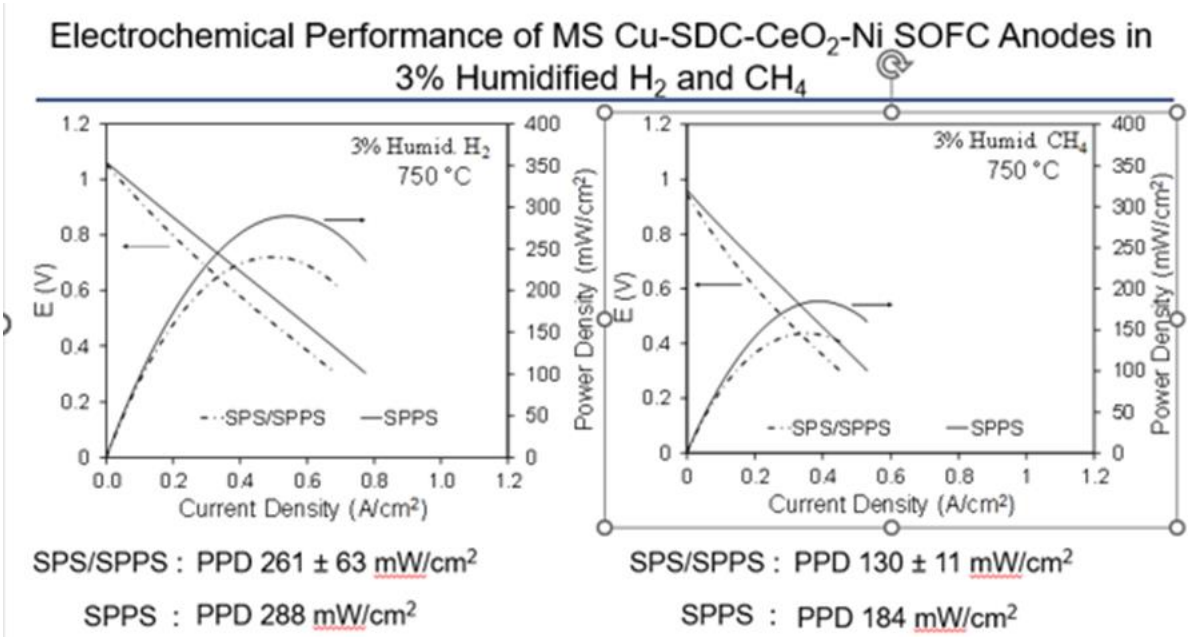

To explore the impact of using alternative fuels such as green CH_4 or natural gas on electricity cost, performance data of MS-SOCs operating on CH_4 were used. For the calculations, the data shown in **Figure 20** were used as the basis of performance estimates.

Performance of the fuel cells fabricated entirely by solution precursor plasma spraying (SPPS) were used, as they achieved better performance than those fabricated by a hybrid method of suspension plasma spraying (SPS) combined with SPPS.

Figure 21 shows the fuel cost of electricity when operating the MS-SOCs on natural gas (NG).

Figure 21 | Fuel cost of electricity for MS-SOCs operating on natural gas

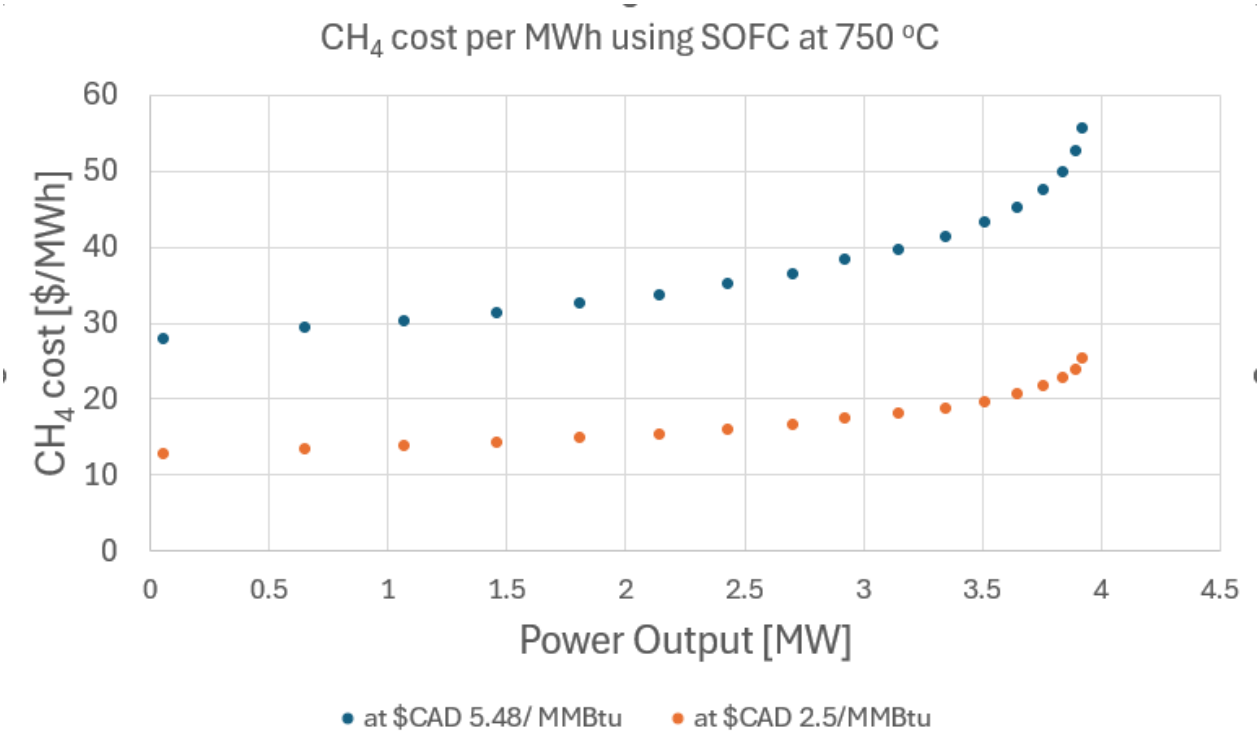

The current cost of NG ($CAD 2.5/MMBtu) and a predicted future cost average over the next 10 years ($CAD 5.48/MMBtu) are both considered. Based on the measured performance data, the fuel cost of electricity for MS-SOCs operating on NG is approximately 10 times lower than that of MS-SOCs operating on H_2. This difference is seen despite the lower performance in CH_4 compared to H_2 due to the lower fuel cost. When using green CH_4 instead of NG, the emissions profile of the fuel would be similar to that of green H_2, while the cost in both cases would initially be higher than the corresponding grey/fossil-sourced versions of H_2 and CH_4 fuels. It is worth noting that an MS-SOC operating on CH_4 produces zero NO_x emissions due to the lower temperature of operation compared to combustion of NG in a gas turbine (GT). Therefore, even when using fossil-sourced natural gas, using it in a fuel cell is a lower-emission way of converting the fuel energy to electricity compared to using it in a GT.

To obtain a fuel cost of electricity calculation for 800 °C using CH_4 fuel, a performance estimate was generated by using the ratio of CH_4 to H_2 voltages and current densities at 750 °C, then multiplying the H_2 performance data at 800 °C by the same ratio. This estimate serves as a first approximation, but a more complete data set including the performance of the MS-SOCs in CH_4 at 800 °C would be required

to obtain higher-precision estimates of the CH_4 fuel cost of electricity at that temperature. Using the ratio of performances in H_2 vs CH_4 at 750 to estimate performance at 800 °C is a reasonable first approximation but not fully precise since the activation energy of fuel cell kinetics using H_2 and CH_4 are not likely to be identical. **Figure 22** shows the fuel cost of electricity for the MS-SOC operating on NG.

Figure 22 | Fuel cost of electricity for an MS-SOC operating on CH_4, using current NG price and future predicted price

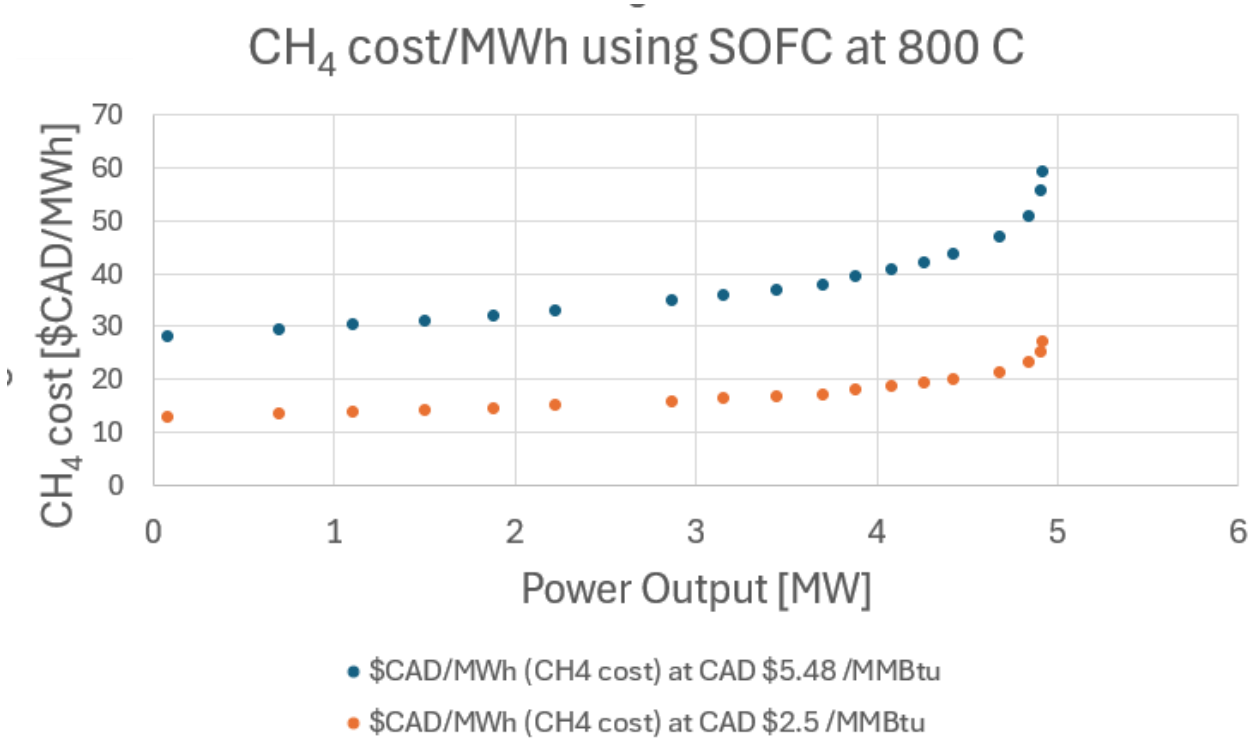

When using CH_4 rather than H_2 for electricity production only (not also for fuel production and storage), the BOP can be less costly, since H_2 compression and storage are not needed.

Since the BOP and stack cost contributions with the hydrogen-based BOP are on the same order of magnitude as the fuel cost, replacing the H_2 fuel cost per MWh with that of CH_4 can provide a conservative estimate of the LCOE, since the BOP for CH_4 would be less expensive if purpose-built. If using the same BOP as with H_2, adding the H_2 BOP cost to the CH_4 fuel costs would produce a reasonable estimate for LCOE.

5.2 Levelized Cost of Hydrogen (LCOH)

Estimates of the energy cost of H_2 and of the levelized cost of hydrogen (LCOH) production use MS-SOC data at 800 °C, shown in **Figure 23**.

Figure 23 | SOC V-I and power density curves for operation in both fuel cell mode (SOFC) and electrolysis mode (SOEC)

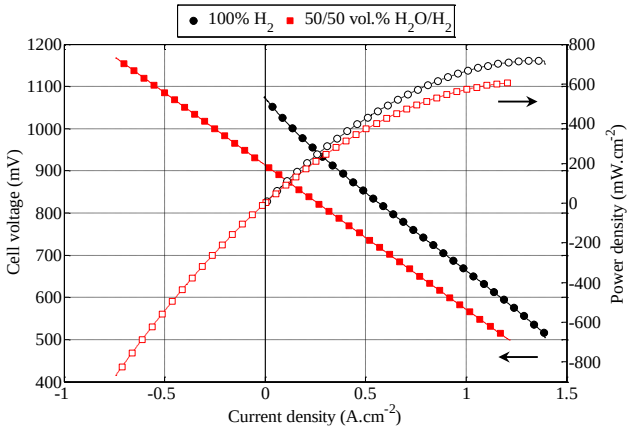

Fuel cell mode data (corresponding to positive current densities) are shown both for performance in dry H_2 and for a 50%-50% volumetric mixture of H_2 and steam. Electrolysis mode data are shown only for the 50-50 mixture of H_2 and steam. **Figure 24** shows how the electrolysis mode performance data in **Figure 23** translate into H_2 production rates and electrical-to-chemical efficiency, for the 50-50 H_2-H_2O feed mixture.

Figure 24 | Performance data of MS-SOCs from Figure 23 translated from voltage and current density to efficiency and H_2 production rates

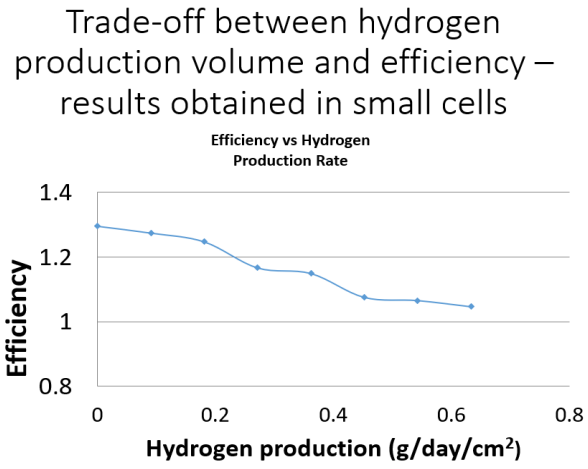

Since the efficiency of an SOC depends on its operating voltage, and the current correlates directly to the reaction rate, the V-I curve can be directly mapped onto an efficiency-hydrogen production curve. The faster the H_2 production rate, the lower the efficiency of the process for a given size of electrolyzer hardware.

One outstanding characteristic of high-temperature solid oxide electrolysis (SOE) compared to low-temperature electrolysis (e.g. alkaline (A) or proton exchange membrane (PEM) electrolyzers) is that both kinetics and thermodynamics of electrolysis improve with increased temperature. In fuel cell mode, kinetics improve with temperature while thermodynamics become less favourable. Since the effect is stronger for kinetics, SOFCs are more efficient than PEMFCs or alkaline fuel cells (AFCs) due to faster kinetics. But SOECs have an even greater advantage over PEMECs or AECs due to their superior kinetics and thermodynamics at the higher temperatures.

In particular, one remarkable feature of high-temperature electrolysis thermodynamics stands out in a surprising way: the electrical-to-chemical efficiency can be greater than 100 % when an external supply of heat is provided. Since at the elevated SOEC operating temperatures, both heat and electrical energy can be inputs into the chemical enthalpy of the fuel that is being produced, an SOEC that is co-located with a free source of by-product heat can use less electricity to produce fuel compared to a low-temperature electrolyzer. Such sources of free by-product heat could include small modular reactors (SMR) being developed for distributed nuclear power generation, for example, or industrial process such as steel or cement production, where both heat and CO_2 that result from the processes could be used for electrolysis. In the scenario where both heat and CO_2 are available, co-electrolysis of CO_2 and H_2O can be utilized to produce syngas, as will be discussed in a subsequent section.

The electricity cost of H_2 production was calculated for several levels of electricity cost, using the data in **Figure 23**, and assuming a 50/50 H_2/H_2O mixture is fed to the SOEC at 800 °C. The water cost contribution was calculated and contributed less than $0.001/kg H_2 at Ontario retail utility rates, and therefore was subsequently not included in this and subsequent H_2 cost analyses. The electricity cost of H_2 production at the conditions described is shown in **Figure 25**.

Figure 25 | Electricity cost of H2 production using SOEC operating at 800 °C

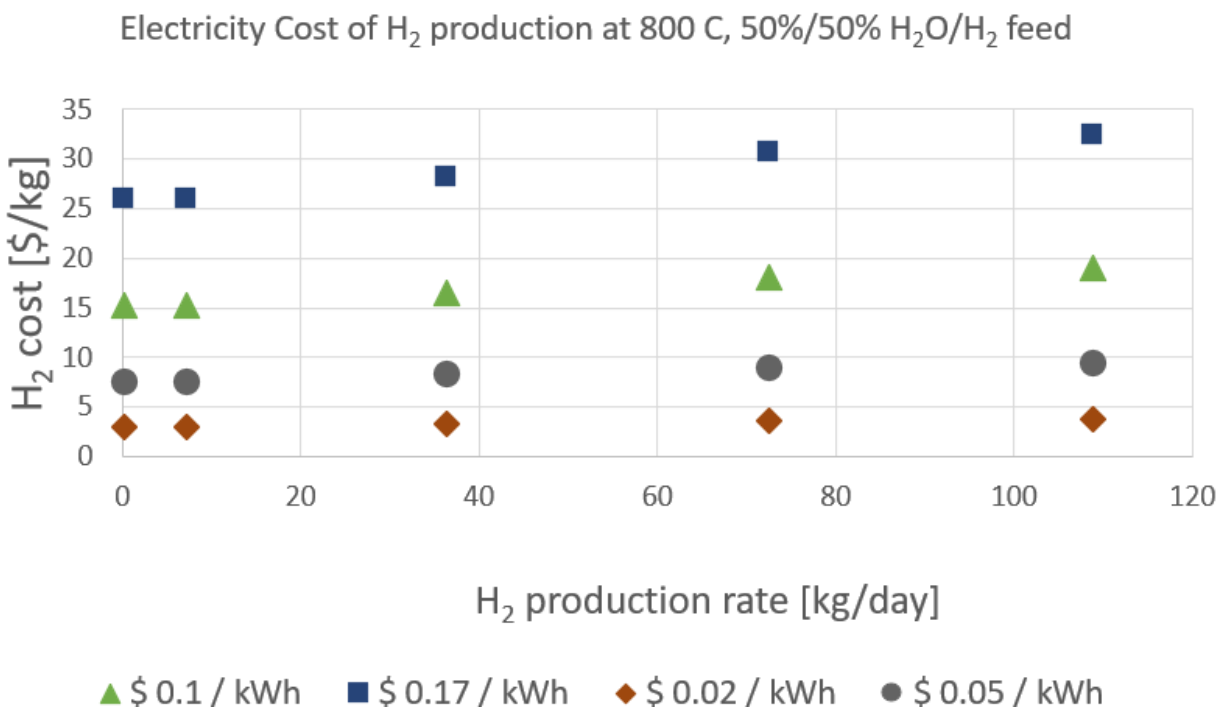

The electricity cost of H_2 production at 800 °C when feeding a 90 vol %/10 vol% H_2/H_2O mixture was calculated based on the available 50/50 H_2O/H_2 data. The voltages at all operating points were adjusted by the calculated difference between the thermodynamic Nernst voltage (ideally mapping to the open circuit voltage) at the two feedstock gas compositions. The results of the calculation are shown in **Figure 26**.

Figure 26 | Electricity cost of H2 production as a function of operating condition and of H_2 cost

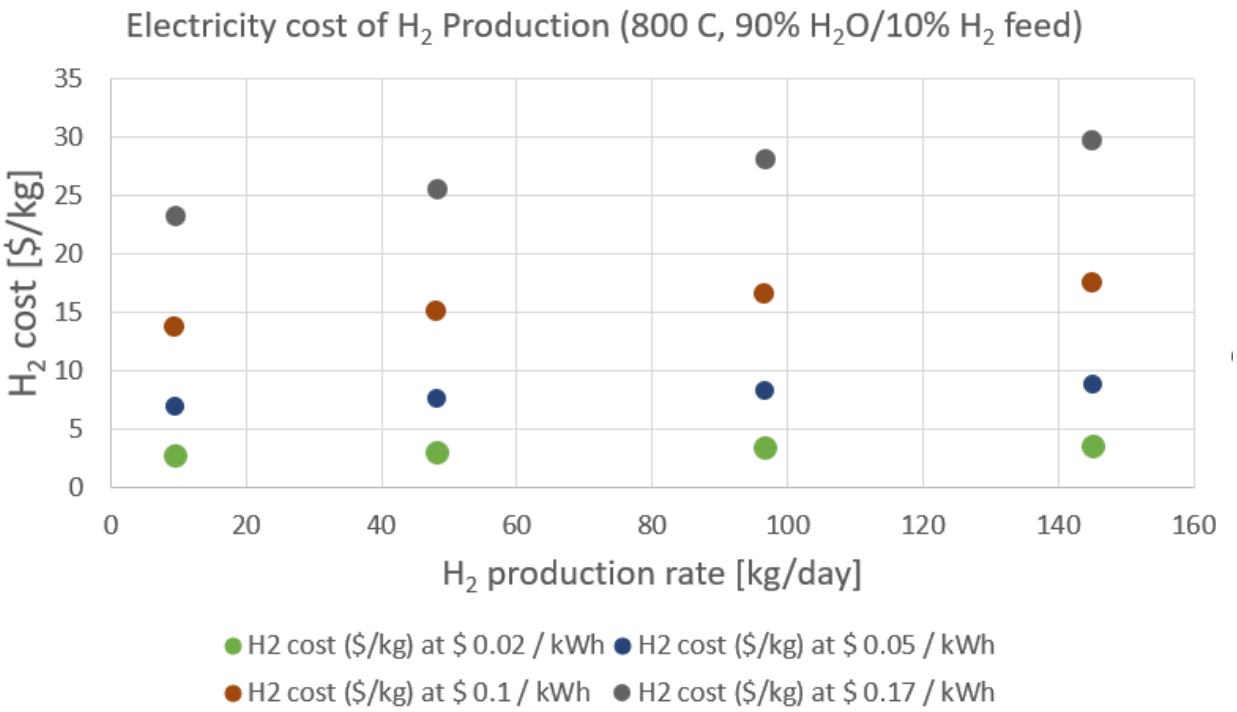

From **Figure 25** and **Figure 26**, it is clear that the H_2 production cost varies strongly with the cost of electricity used for the electrolysis process. It also varies according to the H_2 production rate for a given system size, as the change in production rate changes the efficiency of the process as well, as discussed in relation to **Figure 24**. The electricity cost of H_2 production at both temperatures was calculated for a nominal 5 MW (sized based on SOFC mode) system over the range of operating conditions shown in electrolysis mode. For reference, the average cost of electricity in Ontario in 2023 was $0.0297 per kWh (between our conditions of $0.02/kWh and $0.05/kWh), as reported by Statista Research Department in June 2024.

For the calculation of levelized cost of hydrogen (LCOH), the influence of system size for stack and BOP was considered. For the comparison of system size influence, the MS-SOC systems were assumed to be operating at a voltage of 1.0089 V, which is slightly above the thermoneutral voltage (Vth) of 1.0075 V at 800 °C. At this operating point, the electrical-to-chemical efficiency of the process is very close to 100%, with the 'waste' heat from the inefficiencies in the electrochemical process also being converted to chemical enthalpy of the fuel produced. It is assumed that the built system would be well-insulated to minimize loss of heat to the surroundings, and that the small amount of heat released by operating slightly above Vth may be sufficient to maintain the temperature of the system when it is well-insulated. This assumption is likely to be reasonable in practice after the initial start-up of the

system to reach its operating temperature range is completed, but empirical data will be required to confirm the assumption.

The LCOH is shown in **Figure 27**, for the 90%/10% H_2/H_2O mixture conditions shown in **Figure 26**. The LCOH assumes a 5-year stack life and a 10-year BOP life. As discussed in relation to the LCOE, the 10-year BOP life estimate is likely to be a large underestimate, but the highly conservative lifetime assumption for BOP was chosen to offset the uncertainty in predicting the lifetime of the new MS-SOC technology as 1000-hour durability tests are translated into lifetime estimates for the purpose of LCOH calculations.

Figure 27 | LCOH for an SOEC system operating at 800 °C on a 90/10 mixture (by volume) of H2/H2O, operating very close to and slightly above the thermoneutral voltage

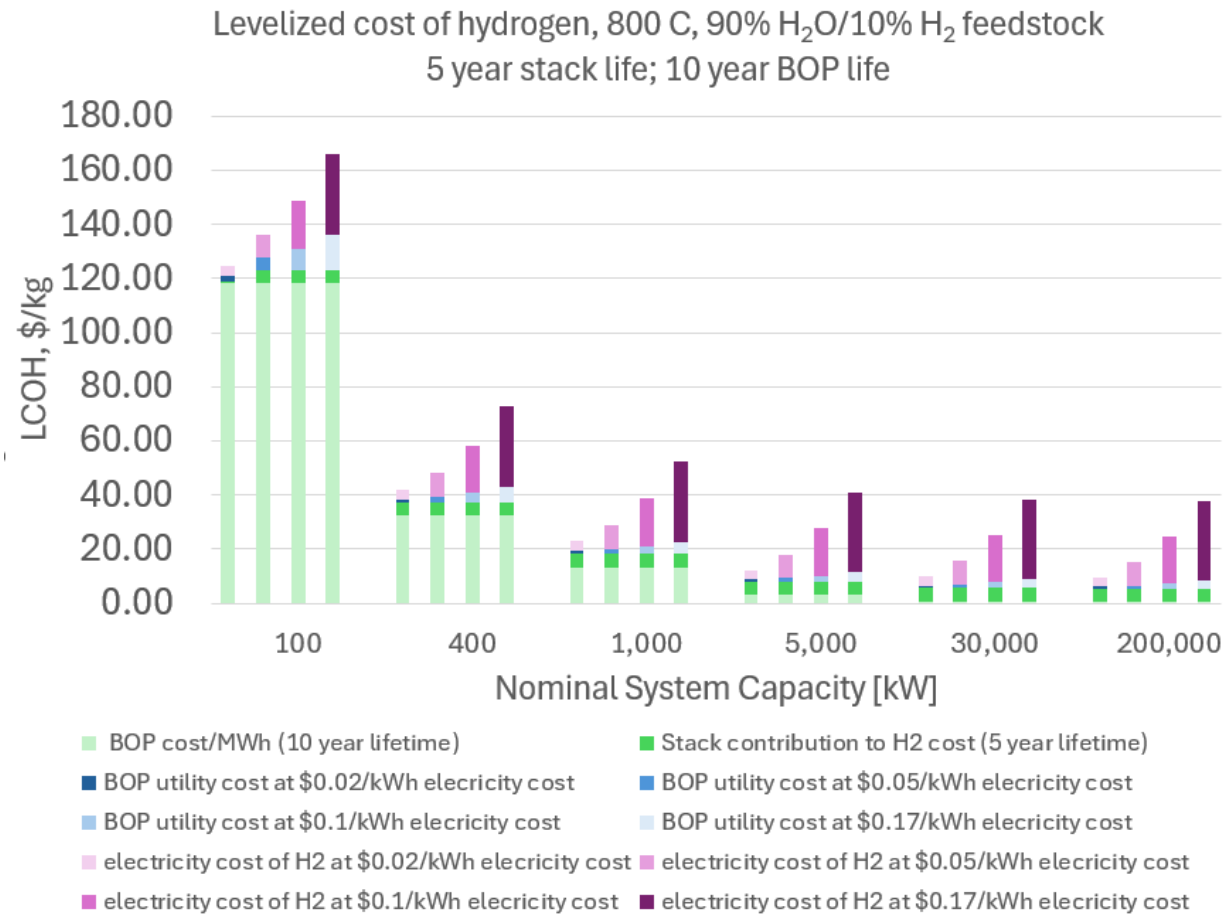

As shown in **Figure 27**, the BOP cost dominates the LCOH for small system sizes, due to the use of 3 stages of compression and drying to fully dry the H_2 that is produced and store it at 750 bar. The hardware required for the BOP is therefore averaged over too-small a H_2 output in the 100 kW system to make the H_2 cost-effective for the 5- and 10-year lifetimes assumed for the LCOH calculations. **Figure 28** therefore shows the same data set as in **Figure 27**, but with the 100 kW system removed to enable easier comparison between the other system sizes.

Figure 28 | LCOH for SOEC operating at 800 °C in 90/10 H_2/H_2O mixture near Vth

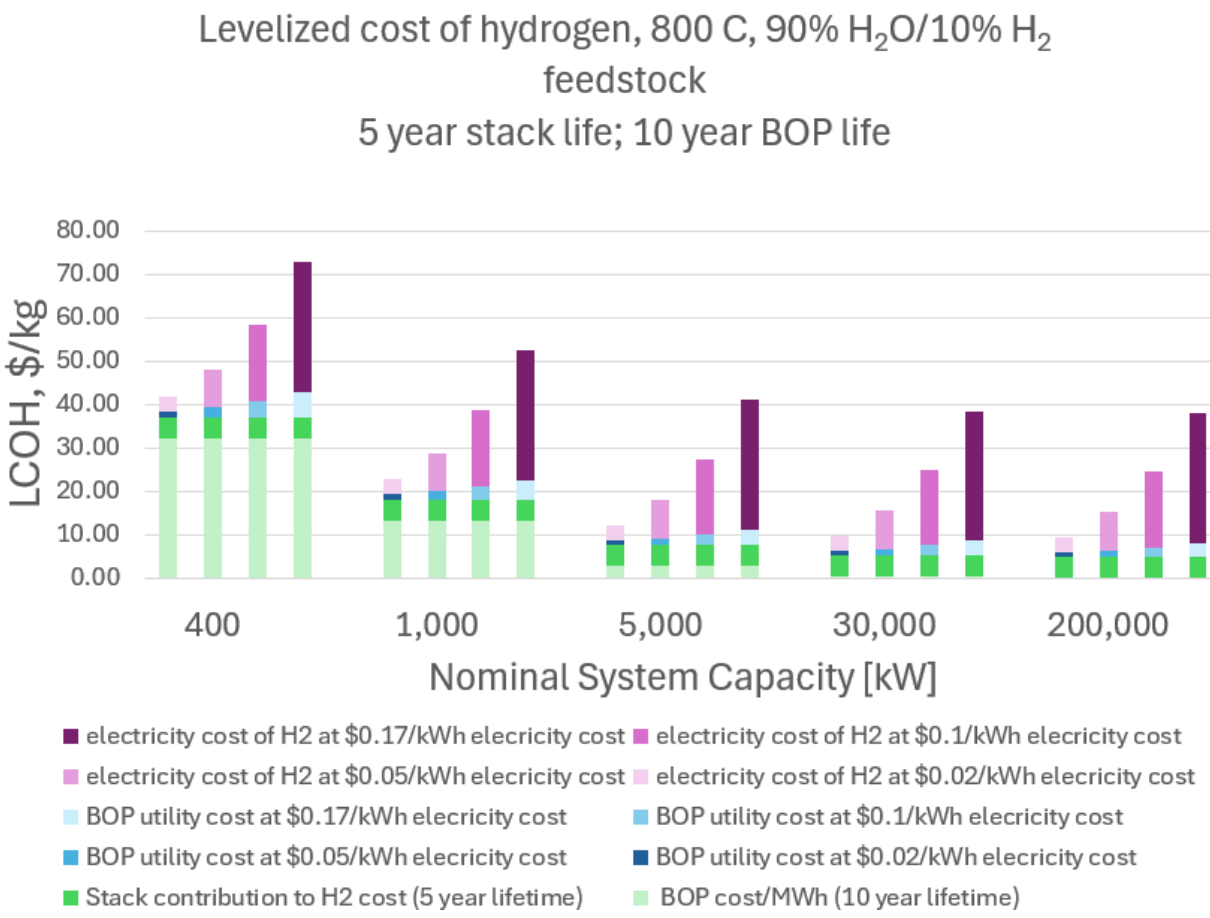

The 10% H_2 in the feed mixture is provided to protect the fuel electrode from oxidation near the electrolyzer inlet, where 100% steam would risk oxidizing the nickel and any other metallic materials in the fuel electrode composite. This is a conventional operational strategy used for avoiding reduction/oxidation (redox) cycling, which can lead to catastrophic failure of the electrolyte in traditional fuel electrode-supported SOFC architectures. In the MS-SOC architecture developed, previous work has shown that redox cycling does not lead to catastrophic failure of the electrolyte as it does in the more traditional designs, so the MS-SOC design is likely to be more robust against failures due to accidental oxidation of the electrode, in situations such as unanticipated fuel supply interruptions. Even so, the 10% H_2 is assumed to be part of the feedstock even in the MS-SOCs, because redox cycles, while not causing failure of the electrolyte in one cycle, can lead to small (~1% performance loss) with each such cycle based on our previous work, so it is deemed preferable to prevent such cycling during standard operation, so that the additional robustness of the MS-SOC design can be reserved for preserving the cell performance in situations where redox cycling is unintended.

5.3 Scenario Specific Levelized Cost

Fueling Station of the Future

While most TEA's for H_2 fueling stations use off-site H_2 production which is delivered in the form or liquid or gas, on-site H_2 production introduces cost savings on fuel transport and logistics while minimizing losses related to H_2 leakage.

An inherent advantage of the MSRSOC lies in its ability to decouple energy generation from demand. By facilitating energy buffering in the form of H_2 or hydrogen-based fuel, MSRSOCs introduce an inexpensive and straightforward way to store energy to reversibly produce power on demand. Unlike conventional energy storage techniques such as lithium-based battery energy storage systems (BESS), which require additional batteries and associated footprint to scale up energy storage, hydrogen-based storage offers an added advantage of coupling a low capacity electrolyzer system to produce H_2 for larger storage over extended time periods, thereby decoupling energy storage from production and occupying lesser footprint.

In this scenario a zero-emission vehicle (ZEV) fueling station comprising a MSRSOC system operating at 25 MW capacity in FC mode to service electric vehicles (EVs) and at 60 MW capacity in EC mode to service hydrogen-based heavy duty (HDV) trucks is considered to introduce a prototype of the MSRSOC technology for energy decoupling. The specifications of the fueling station considered includes 8-10 electric charging stations with 200 kW RSOC stacks operating in FC mode with each stack having the ability to service one 50 kWh capacity EV car every 15 minutes. The RSOC operated in EC mode is equipped to service 2 hydrogen-based HDVs requiring up to 70 kg of H_2 each. The fuel station is designed to possess an H_2 storage capacity equivalent to 150 MW-h of energy and is designed to operate continuously for 66 hours over a period of 3 days with 6 hours allocated to H_2 refueling through electrolysis. **Figure 29** depicts the MSRSOC based ZEV fueling station concept.

Figure 29 | Conceptual schematic view of a MSRSOC based ZEV fueling station

The total installed capital cost of the MSRSOC system is evaluated based on the total manufacturing cost of the technology, cost of installed BOP and cost of H_2 storage based on a commercially available Type-IV 450 bar cylinder with a capacity of approximately 250 kg per skid as indicated in Appendix 3. **Figure 30** illustrates the H_2 storage cylinder and footprint utilized by the designed MSRSOC system.

Figure 30 | Schematic view of Type IV portable skid-based H_2 storage cylinders

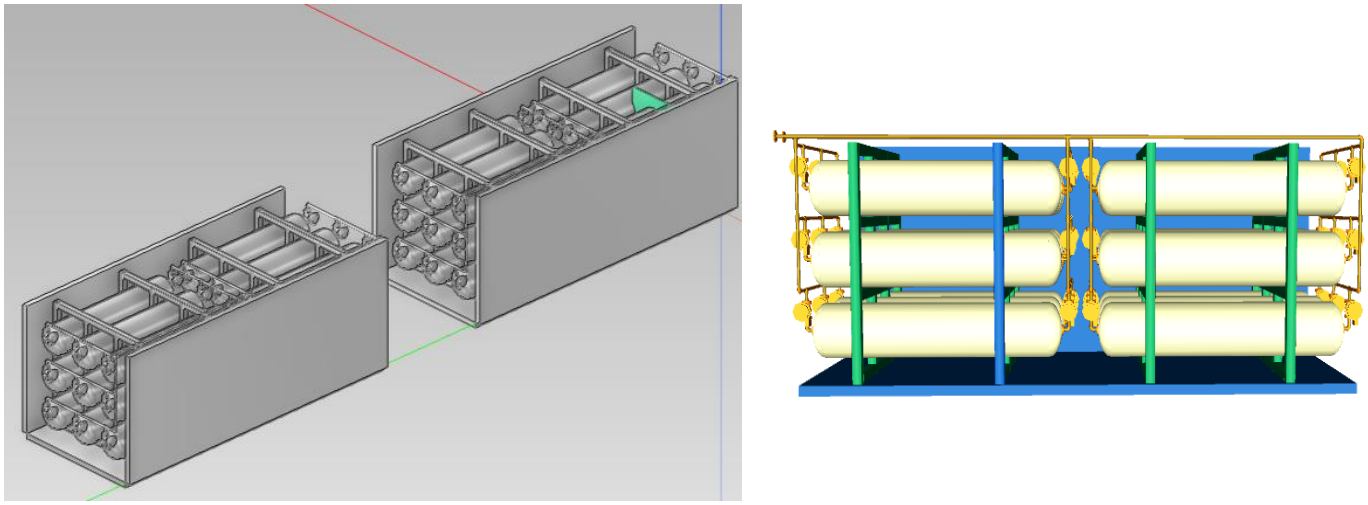

Table 2 | Table showing total installed cost of SOC vs Tesla Mega Pack

Technology	Down-time (hours)	System Capacity [MW]	Storage Capacity [MW-h]	BOP Cost [millions USD]	System Cost [millions USD]	# of energy storage units	Storage Cost [millions USD]	Total installed cost, [millions US$]
SOC	6	25	150	$17	$4	18	$2	$23
Tesla Mega Pack	4	38	153	N/A	N/A	39	N/A	$52

Table 3 | Table showing total installed cost per kW for SOC vs PEM

Technology	Refueling time (hours)	System Capacity [MW]	Total Installed Cost per kW [US$]
SOC	6	60	$600 - $800
PEM	6	60	$700

To test the SOCRATES concept in real life scenarios, IESO Hourly Ontario Energy Price (HOEP) data

for the months of January and May was obtained and plotted. These two months were chosen to represent two scenarios for electricity prices, the winter price in January and spring price in May. As can be seen the below figures the price average price of electricity in January (**Figure 31**, **Figure 32**) is significantly higher than that of May (**Figure 33**, **Figure 34**). For the SOCRATES concept since only 6 hours of H_2 generation is required every 72 hours, we selectively chose strategic blocks of either 6 continuous hours or 2 blocks of 3 hours every 72 hours for the entire month. Based on these electricity prices, we estimated a levelized cost for H_2 production based on 10-year BOP, and 5 year stack life for H_2 production every 6 hours in a 72 hour period assuming the electrolyzer operates at its highest efficiency point at thermoneutral voltage. We obtained a very competitive price of less than $5/kg of H_2 produced.

Figure 31 | Real Time HOEP for Month of January

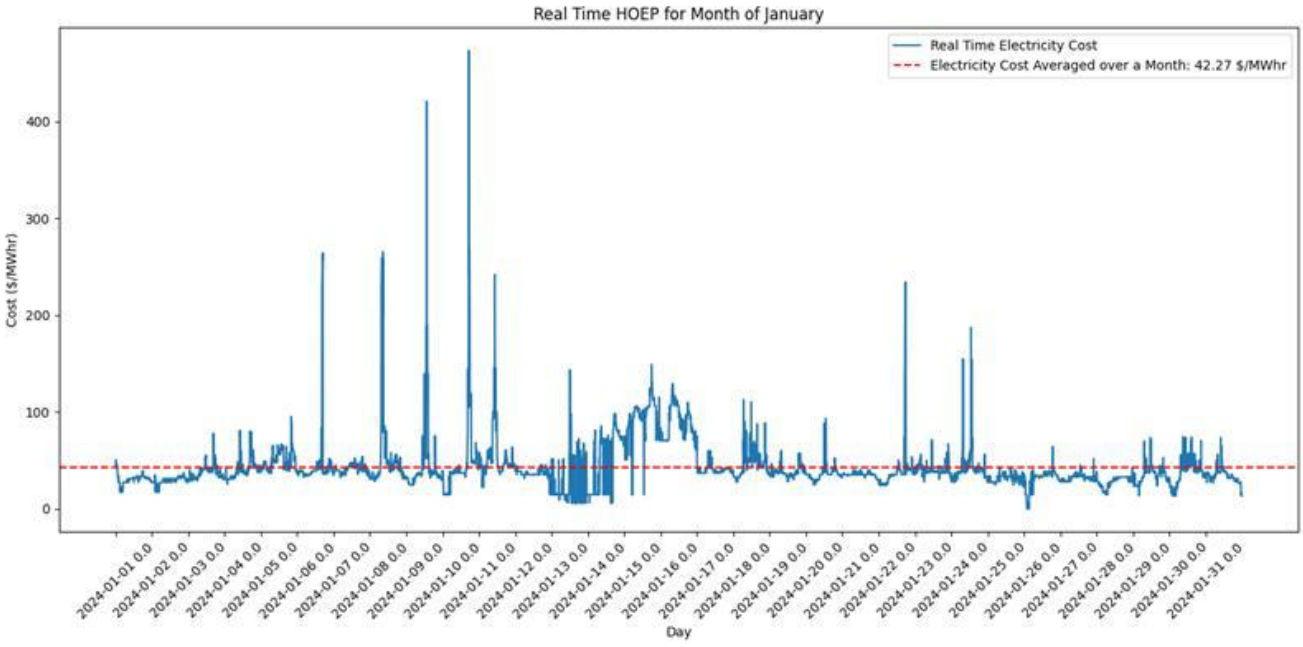

Figure 32 | Selective 6 Hours for Opportunistic H_2 Production Every 72 Hours for Month of January

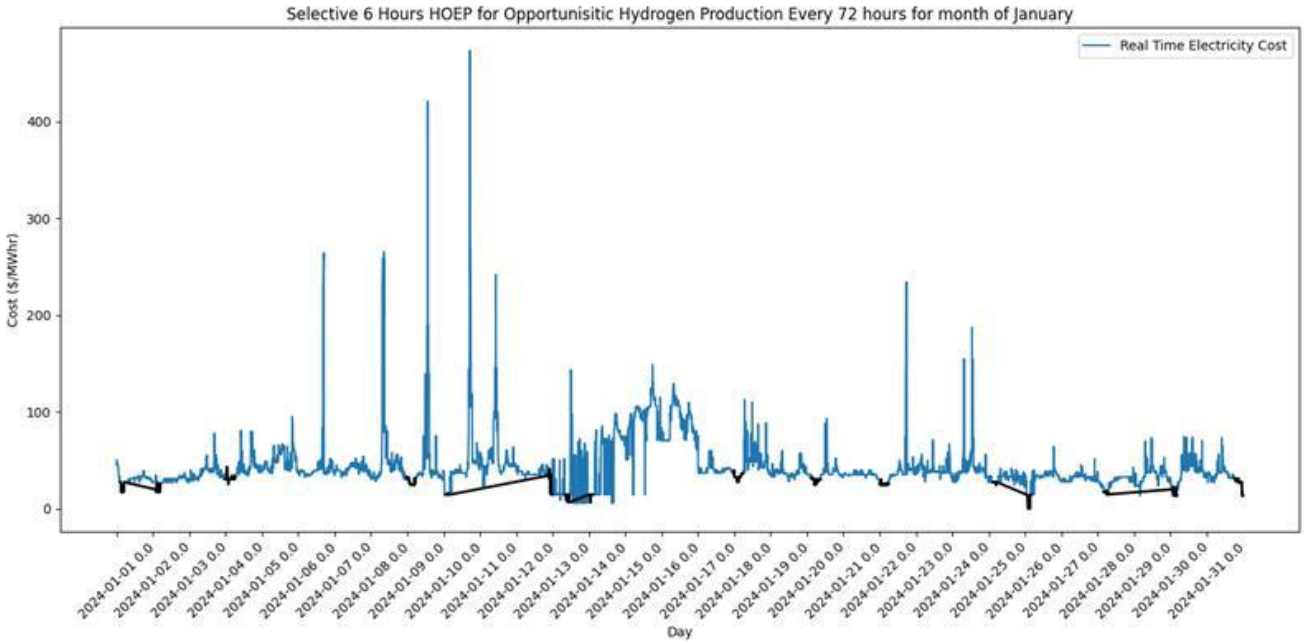

Figure 33 | Selective 6 Hours for Opportunistic H_2 Production Every 72 Hours for Month of May

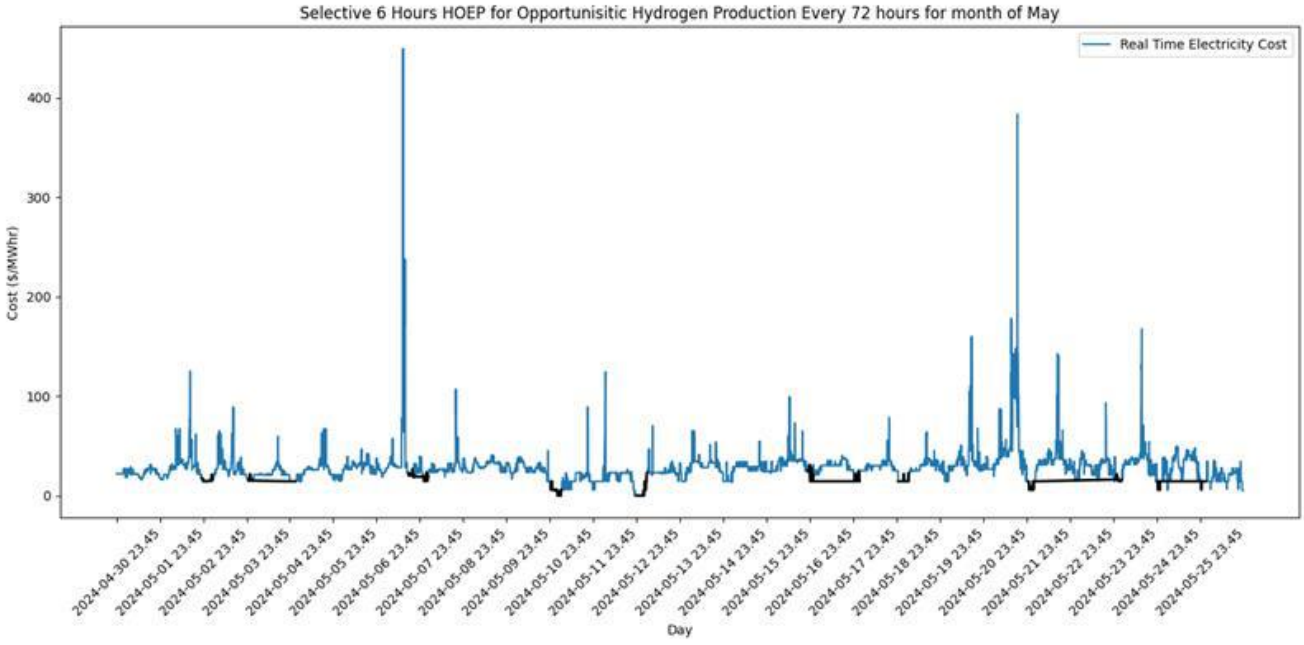

Figure 34 | Real Time HOEP for Month of January

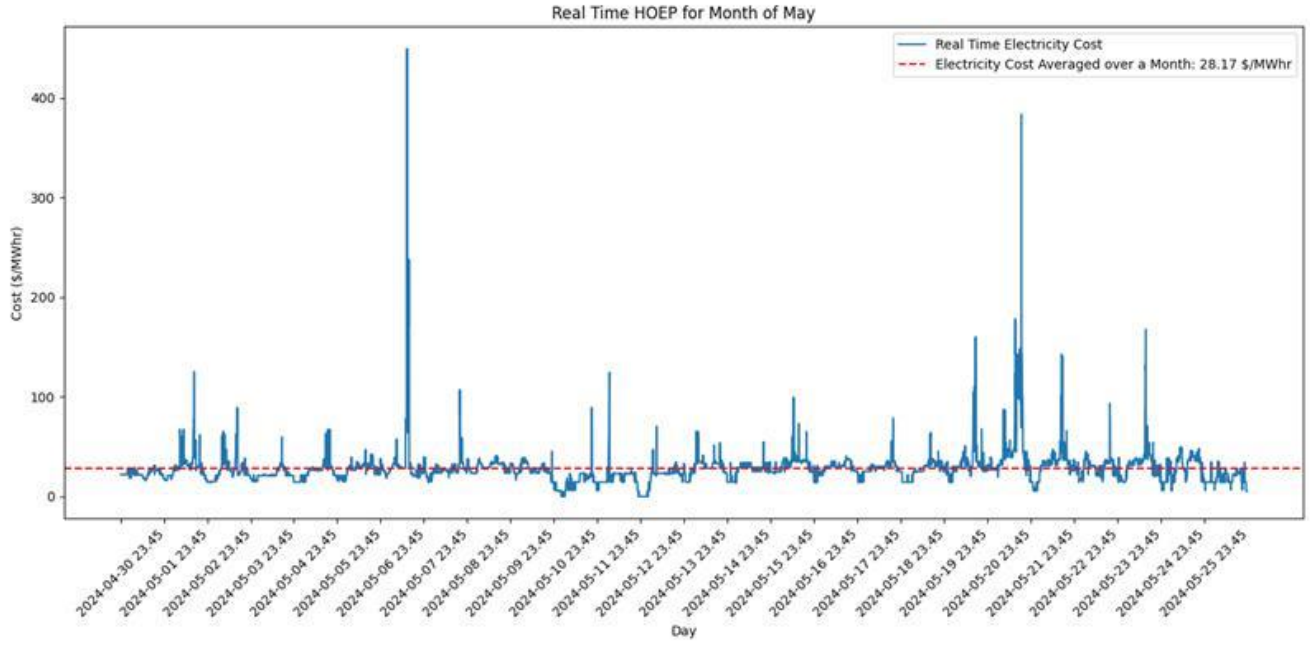

Table 4 | Selective 6 Hours HOEP for Opportunistic H_2 Production Every 72 hours for the month of January

Date Range	Interval Length (Hours)	Selective Cost ($/MWhr)	Cost of H_2 Produced ($/kg)
2024-01-01 to 2024-01-03	2x3	21.54	3.85
2024-01-04 to 2024-01-06	6	31.23	4.12
2024-01-07 to 2024-01-09	6	27.52	4.02
2024-01-10 to 2024-01-12	2x3	21.28	3.84
2024-01-13 to 2024-01-15	2x3	13.92	3.64
2024-01-16 to 2024-01-18	6	32.80	4.17
2024-01-19 to 2024-01-21	6	29.44	4.07
2024-01-22 to 2024-01-24	6	25.15	3.95
2024-01-25 to 2024-01-27	2x3	17.33	3.73
2024-01-28 to 2024-01-30	2x3	15.73	3.69
2024-01-31 to 2024-01-31	6	26.82	

Table 5 | Selective 6 Hours HOEP for Opportunistic H_2 Production Every 72 hours for the month of May

Date Range	Interval Length (Hours)	Selective Cost ($/MWhr)	Cost of H_2 Produced ($/kg)
2024-05-01 to 2024-05-03	6	15.35	3.68
2024-05-04 to 2024-05-06	2x3	14.90	3.67
2024-05-07 to 2024-05-09	2x3	19.32	3.79
2024-05-10 to 2024-05-12	6	4.33	3.37
2024-05-13 to 2024-05-15	6	3.97	3.36
2024-05-16 to 2024-05-18	2x3	18.61	3.77
2024-05-19 to 2024-05-21	6	15.09	3.67
2024-05-22 to 2024-05-24	2x3	11.81	3.58
2024-05-25 to 2024-05-26	2x3	13.44	3.63

5.4 Use of Electrical Energy to Produce Hydrogen for Export

To calculate the quantity of H_2 that could be produced for export using renewable energy, a direct calculation was made of the amount of H_2 that could be produced from electrical energy, if sufficient SOEC capacity is available. The operating condition for the calculations is assumed to be at the thermoneutral voltage (Vth) for solid oxide electrolysis, a condition at which the electrical-to-chemical efficiency is 100%, and no additional heat input is required. Operating below Vth would allow for some additional available heat to also be incorporated into the produced H_2 fuel enthalpy, thus partially offsetting some of the electrical energy required. But it would also require locating the system adjacent to the source of free heat. Since it is most likely that the H_2 production would be geographically distributed, it was not assumed that any of the systems had access to external free heat, and therefore, that all of the chemical enthalpy of the H_2 fuel is supplied via electrical energy. At the thermoneutral condition, a significant H_2 production rate is possible even with 100% electrical-to-chemical efficiency. If a faster production rate is required, more H_2 can be produced at a trade-off of using more electrical energy per kg of H_2. For comparison purposes, low-temperature electrolysis at temperatures close to 100 °C, as used in Proton Exchange Membrane Electrolysis Cells (PEMECs) or Alkaline Electrolysis Cells (AECs), cannot achieve the 100% electrical-to-chemical efficiency conditions at that temperature. Low-temperature electrolyzers typically operate at electrical-to-chemical efficiencies of approximately 75% based on the higher heating value of the H_2 fuel being produced.

Thus, comparing high-temperature SOECs vs. low-temperature PEMECs or AECs, the same installed electrolyzer capacity and energy input would produce 33% more H_2 in an SOEC system than in either of the low temperature systems.

Both types of electrolyzers can utilize geographically-distributed renewable energy to produce H_2 in local or self-contained electricity systems, since both types of electrolyzers are modular, and retain their high efficiencies even at small-scale fuel production, making them suitable for use as part of an energy storage infrastructure that can be widely distributed and used where needed. PEMECs are more widely commercialized to date, having been in development for decades prior to the development of SOECs. However, due to the higher efficiency of SOECs (as well as their fuel-flexibility to produce syngas as well as H_2 via electrolysis with renewable electricity), SOEC development is rapidly underway to close the gap in utilization between the two technologies. MS-SOC technology in particular is anticipated to be especially well-suited to opportunistically make use of otherwise curtailed power that becomes available at unpredictable times, such as wind power, due to its combination of rapid start-up capability (shared with PEMECs) and high efficiency (shared with traditionally designed SOECs).

6. Conclusion and Recommendations

This project has achieved the following:

1. Established the feasibility of using the developed cell components in scalable reversible SOC's capable of rapid response in electrolysis or fuel cell mode.
2. Provided insights into the performance capabilities of our technology to provide grid services, support intermittent generation and load following in response to grid demand.
3. Evaluated short term, seasonal and long term storage of H_2, and proposed technological pathways for carrier fuel conversion and decarbonization potential for the same.
4. Identified the road map for continuing work on technology development and the factors that will impact the success of the same. This includes technological breakthroughs required as well as economic factors associated with costs, barriers and regulatory regimes.
5. Power generation through H_2 using fuel cells should be a part of future planning

6.1 SOC Cell Component Work

The main findings of this project related to SOC components include the development of an improved tape casting procedure that produces flat components from a stable aqueous suspension of steel particles. Overcoming the challenge of uneven drying of aqueous tapes will make it more feasible to scale up the area of the cells, and important next step towards commercialization. The project also resulted in a new sintering strategy that significantly lowers the surface area of porous steel support structures compared to the previous strategy of using fine powder to prevent large surface pores that lead to electrolyte defects. This improvement will increase the longevity of metal-supported cells by decreasing the rate of chromium loss caused by growth of chromium oxide layers on the surface of the stainless steel. The project also resulted in support structures with 4.5 times higher gas permeability than the commercially-available substrates previously used, and higher permeability than the in-house support layers developed prior to the project, while simultaneously decreasing the surface area of the structures. This improvement is expected to lead to improvements in cell performance, both short-term due to higher mass transport, and long-term due to the increased time available before the pores would fill with excessive oxide growth. Modified processes using the application of a magnetic field to align the ferritic stainless steel particles, of freezing to create aligned ice crystals that result in aligned porosity after sublimation, and a combination of both were also developed. These substrates were found to have even lower surface area than the ones produced with the modified sintering strategy due to the straighter and more aligned porosity; this change in turn is expected to further extend the lifetime of the components.

It was also determined that idling the stack at high temperatures in dry CH_4 should be avoided. This result is in part due to the possibility of irreversible damage when carbon is not actively being removed by steam and by oxide ions during cell operation, but primarily because other component materials in the balance of plant, such as components made from aluminum oxide or from stainless steel, can also undergo damage from carbon deposition when there is no steam available to gasify

the carbon shortly after it is deposited. Therefore, idling conditions for a system that is intended to operate intermittently for load following applications should either involve a carbon-free atmosphere to be maintained in the fuel compartment of the cells (e.g. H_2 or a mostly-nitrogen atmosphere with small amounts of H_2), or a lower temperature for idling should be maintained.

6.2 SH2

In terms of this study, the development of mathematical models and associated controls for SH2 has been a successful first step in the engineering of SOCs as complete systems, ready for practical use. While we have shown that the use of suitable controls can greatly benefit SOC performance, more advanced control theories and robust control strategies are likely to improve performance. In addition, advanced robust or adaptive controls may lead more resilient realizations of SOC stacks. Our simulations demonstrated basic operation of controlled SOC stacks, but we recommend performing studies with system perturbations (like ground faults or loss of communications with critical infrastructure), to assess the practical potential of this technology in harsh realistic environments.

Apart from the SOCs as stacks onto themselves, we recommend extensive studies of the interaction of controlled SOCs within realistic power grid systems. For example, while we have shown that an SOC can, in principle, support the operation of a single electric power generator, what sort of complex interactions might emerge as greater numbers of SOCs (possibly on the distribution side of the grid, supporting various microgrids), as well as traditional bulk-power generators, are incorporated? Simulation tools are available (such as Simscape Electrical or PS-CAD), which would allow additional investigations of power systems incorporating SOCs.

6.3 Hydrogen Carrier Fuel Pathways and Decarbonization

As detailed in Appendix 3, because of the unique characteristic of H_2 molecules, being of diatomic structure with the lightest and smallest atoms, H_2 has high extremely low boiling point (- 252.9 °C), low density, volume energy density, and high diffusivity. Any attempt to liquefy H_2 gas is a process of energy intensive and thus with low net energy efficiency, furthermore, H_2 gas can diffuse through metals, resulting in "hydrogen embrittlement".

Therefore, even though H_2 is a promising green energy, it presents challenges in its storage and transportation. Cylinder/tanks storage is suitable for short-distance transportation and small-quantity of H_2 storage; blending H_2 gas with natural gas serves as a practical method for short-term H_2 storage and transportation. For long-term storage and transportation, a practical way is to convert H_2 into carrier fuels, such as CH_4 and methanol for industrial use. Our calculations have confirmed that transforming H_2 into CH_4 and methanol has energy conversion efficiencies of 81%, and 84%, respectively, with benefit of utilizing captured CO_2. Note, for methanol energy conversion efficiency calculation, we assumed that Volta Energy catalysts will facilitate the reaction successfully at 170 °C.

Converting H_2 gas to carrier fuels not only serves as a long-term H_2 storage but also a decarbonization pathway, because the processes of the conversion utilizing the captured CO_2. The following **Figure 35** highlights the decarbonization pathways.

Figure 35| Pathways for Green H_2 Production and CO_2 Utilization/Decarbonization Facilitated by Reversible SOC

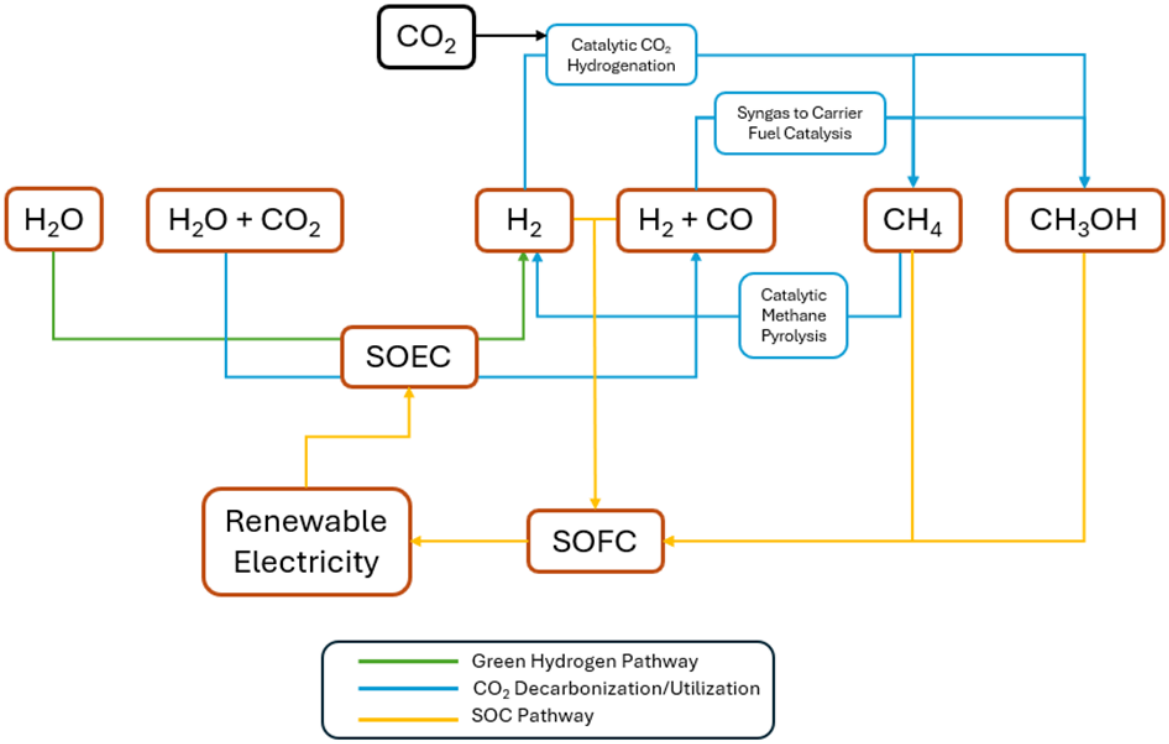

Both the processes of converting H_2 gas along with captured CO_2 to CH_4 and methanol are decarbonization pathways.

When methanol is used as a fuel for SOFC to generate electricity, CO_2 is produced. However, the released CO_2 can be captured and reused to make H_2 carrier fuels, as outlined in the green H_2 production pathway (**Figure 35**). When methanol is decomposed, it will produce CO and H_2, making syngas, a valuable raw material for manufacturing various fuels.

Our calculations indicate that 1.37 tonne of captured CO_2 is utilized for every tonne of methanol produced through either direct CO_2 hydrogenation or syngas pathway, and 2.74 tonne of captured CO_2 is utilized for every tonne of CH_4 produced. In addition, CH_4 pyrolysis also serves as a unique decarbonization pathway, as it indirectly converts CO_2 into solid high value carbon material, a negative CO_2 emission pathway. Our studies demonstrate that CH_4 pyrolysis can be achieved at 500 °C when using the catalyst developed by Volta Energy, producing twice the stoichiometric and one times the stoichiometric amount of H_2 gas and carbon nanomaterial, respectively, from CH_4.

All the processes—methanation, methanol production, and CH_4 pyrolysis—require effective catalysts for efficient transformation. Volta Energy has designed and synthesized catalysts for these processes, and thorough characterization and initial reaction tests have shown them to be promising for the intended reactions.

6.4 Techno Economic Analysis

The TEA has provided levelized costs for both H_2 and electricity production in a variety of scenarios. We have established the economic feasibility of MSRSOC technology with larger capacities based on our developed Balance of Plant. We have shown the application of this technology in the context of targeted projects for grid buffering and fuelling stations of the future.

7. Lessons Learned

This project was big in scope and completed under a very aggressive schedule. This project was also unique in that it combined experimental work with theoretical modelling along with detailed techno-economic analysis. This project offered several lessons learned from a technical as well as a project management perspective. Some of the significant ones have been highlighted below.

1. Limit the scope of work

This project had a massive scope and, although necessary to establish the "lay of the land" for systems based on MSRSOCs, coordinating the disparate interdisciplinary activities was a huge challenge in 10 months. For future projects, some siloing is needed for greater team focus and milestone completion. At this point, our focus is on depth rather than breadth as we develop and prototype the essential constituent technological parts.

2. Risk analysis on critical path project activities - unforeseen delays in lab facilities

The renovation plans at the University of Toronto's Plasma Spray Lab were scheduled to be complete according to the original schedule by December 2023. Unfortunately, due to supply chain constraints, the renovations were not completed. Following good project management practices, we had a contingency plan which we reverted to which involved outsourcing the work to a commercial lab in British Columbia. Coordination with the third-party lab did require some additional time (and cost). In retrospect, we should have coordinated with the outside plasma spray facility prior to the beginning of this project. Overall, the lesson learned is for aggressive schedules even small unforeseen delays can have significant impacts and a detailed risk analysis should have been done at the beginning of the project for the critical aspects.

3. Additional computational resource for computationally intense simulations

For both SOC modelling using FEA and SH2 simulation (particularly with three-phase power devices), iterations took much longer than expected, owing to the complexity of the models. More capable computing systems including faster processors (for example, multi-core or GPU-equipped systems), greater quantities of fast (e.g., DDR5) RAM, would have been helpful to speed development/optimization.

4. In depth awareness of provincial permitting and licensing regulations

Based on our interactions with other entities active in the hydrogen space, one key factor that was noticed was the difference in regulation in permitting requirements based on geographical location of project deployment. Since our project primarily dealt with technical and economic factors, this was one consideration that was not factored in our project scope. For all projects resulting from the results of this project, this factor will be addressed.

8. Next Steps

One of the main goals for upcoming work is to scale up the area of the cells while maintaining sufficient flatness to ensure good electrical contact and while retaining or exceeding the performance achieved with smaller fuel cells. This work requires design and fabrication of hardware for the processing, handling, and testing of the larger cells, from the fabrication of the structural support layer to the manufacture of the fuel cell/electrolysis cells on top of the support layer. The improved microstructures developed in this project will be combined with the application of protective coatings to further decrease the rate of oxidation of the metal supports, thereby further increasing the lifetime of the cells. Fuel cell and electrolysis cell testing also must be performed on the metal support structures with improved microstructures developed in this project to quantify the change in performance that results from the improvements made. Idling conditions should also be tested at various temperatures to determine the effect of carbon deposition at a range of temperatures for new electrode materials that are resistant to damage from carbon deposition during fuel cell operation conditions, which are less severe than idling conditions.

Additional work will be pursued to determine whether carbide ceramic materials can be utilized as the mechanical support structure for SOCs rather than stainless steel. The ability to use MAX phase carbides would provide additional oxidation resistance while maintaining good thermal conductivity and electrical conductivity, but the manufacturing of MAX phase materials is more challenging than for stainless steel, due to the very high fabrication and sintering temperatures needed, and the difficult to achieve the pure MAX phase materials with no extra impurity materials. For both the air and fuel electrodes, higher-performance materials that use ceria-based composites rather than zirconia-based will be explored. Fabrication of ceria using plasma spraying is more challenging than for zirconia due to the small difference between the melting temperature and boiling temperature of ceria, so additional R&D is required to make that material change while maintaining the high deposition efficiencies that we have previously achieved for zirconia.

Finally, we need to refine our electrolyte fabrication process to achieve high-temperature and high-velocity handling of the substrates during the electrolyte deposition process in order to simultaneously achieve electrolyte layers that are both highly dense (low porosity) and crack-free. These two microstructural requirements have in the past been traded off when using plasma spraying as a fabrication method. We have built a prototype substrate handling device to achieve both high temperature and high velocity in the deposition of zirconia-based electrolyte coatings, but it requires modification, and the fabrication process to deposit ceria-based electrolytes remains to be developed.

For the SH2 scope as mentioned in the previous section that apart from the SOCs as stacks onto themselves, we recommend extensive studies of the interaction of controlled SOCs within realistic power grid systems. We plan to pursue this as part of our gridWISE project mentioned subsequently. The catalyst development work will continue with gusto as mentioned below.

Future projects following on our project should focus on the following to develop a more comprehensive outlook from the TEA done in this project:

- Regulatory hurdles for water usage permits
- Zoning for H_2 storage
- Practical H_2 transportation issues
- Potential for removal of subsidies for H_2 based on change in government at federal and provincial level
- Impacts of the federal H_2 Project tax incentive.

Finally, the work completed as part of this project has laid the foundation for many productive avenues of research:

- ISOCHORES (Integrated Solid Oxide Cell Hydrogen Or Renewable Electricity System)

Solid oxide cells (SOCs) operate at extremely high efficiency in electrolysis mode to produce H_2, and in fuel cell (FC) mode they produce electricity from H_2 at higher efficiency than any other FC. Their high round-trip efficiency makes SOCs an excellent candidate for renewable energy storage. Because power and energy can be scaled separately with a FC/electrolyzer system, the technology is well-suited for distributed generation of H_2 and electricity in remote/rural installations and large urban power plants.

The SOCs targeted will also be capable of using natural gas (NG) without reforming it, at higher efficiency compared to reforming. Since the NG is electrochemically oxidized, no NO_x or particulates form, and the high efficiency results in lower CO_2 emissions compared to other modes of utilizing NG to produce electricity. The ability to efficiently use NG allows SOC systems to be deployed right away in FC mode to produce electricity in locations where NG is available in excess, even to the point of being flared as a waste product in some remote oil and gas operations. The same system, without any modification to the SOCs, can also produce and utilize H_2, creating an incentive to build out H_2 infrastructure further.
The SOCs targeted in this work can be cycled on and off within minutes and can be used many times due to both the new cell architecture and robust control system that will be further developed. Therefore, they can rapidly adapt to changes in availability/demand of electricity/H_2. In contrast, most SOCs require hours to be turned on, and some with non-reusable seal designs can only be used once. Future work will also further develop our rapid, cost-effective fabrication technique and build a prototype of the complete system.

- SOCRATES (Solid Oxide Cell-based Reversible Advanced Transportation Energy System)

Reversible SOC based system to provide reliable always available charging of battery or fueling of H_2FC/ICE vehicles using clean fuels (H_2/low CI fuels). The project advances SOC technology to enable remote, scalable, and cost-effective access to clean fuels to support ZEV on-road transportation.

- gridWISE

Terrestrial power grids are increasingly demonstrating a need for buffering to contend with the proliferation of intermittent high demand distribution side loads reflected by the trend toward greater electrification. At the same time, distributed generation including renewable sources and microgrids is becoming more prevalent, increasing complexity of the power grid and complicating grid stabilization, particularly at times of high power demand. The Distributed Energy Resources (DER)

and Management (DERM) paradigm is fundamentally changing the grid infrastructure to a more decentralized architecture. To address these challenges, Volta Energy is developing gridWISE smart energy control and storage solutions for reliable microgrid design. The gridWISE platform consists of IoT-enabled sensing and control embedded hardware (derived from the hardware developed by Volta Energy for its Insite enterprise), advanced power system control and machine learning algorithms, an energy storage module (utilizing SOC technology), an electrical power generator with excitation control, as well as various smart switching elements for protection and control. When used in combination these components provide a foundation for a microgrid that allows back-up power as well as distribution-side power system stabilization to allow for non-disruptive integration of DER into the broader provincial power grid.

- CO_2 utilization for Methanol Synthesis

Volta Energy is further pursuing Methanol production through direct CO_2 activation pathway. In partnership with Prof. Hui Wang at the University of Saskatchewan and the Synchrotron facility operated by the Canadian Light Source, we are proposing a 3-year project for funding by NRCan. The foundational work for this methanol project had been completed through the HIF project; and a significant section of the methanol project will focus on low Carbon Intensity Hydrogen being sourced through technology that has been developed as part of this HIF project. NRCan has accepted Volta Energy's Expression of Interest for the methanol project through their Carbon utilization call and we will be submitting a full proposal in July 2024 with the aim of approval and project kick-off by October 2024. For the methanol project, we are signing an MOU with a Calgary-based contract chemical manufacturer; this project will offer a major decarbonization pathway.

- Highly efficient CH_4 pyrolysis for H_2 and high value carbon recovery

CH_4 pyrolysis is a decarbonization pathways that converts CH_4, which can be produced directly from CO_2, into solid high-value carbon material in addition to H_2 gas. This pathway serves two purposes simultaneously. A patent memo has been filed based on this work. The work will be shared in the coming 2024 Biogas (west) conference in Vancouver, BC, Cananda, and 6th international catalysis and chemical engineering conference –2025 CATCHEM, which will take place in March 2025 in the Netherlands.

9. References

[1] D. Zhou and R. Vassen, "Thermal barrier coatings manufactured by suspension and solution precursor plasma spray—State of the art and recent progress," in *Thermal Barrier Coatings (Second Edition)*, H. Guo, Ed., in Woodhead Publishing Series in Metals and Surface Engineering. , Woodhead Publishing, 2023, pp. 199–228. Accessed: Aug. 20, 2024. [Online]. Available: https://www.sciencedirect.com/science/article/pii/B9780128190272000110

[2] "Development of Bi-layer Metal Substrate Architectures for Suspension Plasma Sprayed Solid Oxide Fuel Cells - Arevalo-Quintero - 2018 - Fuel Cells - Wiley Online Library." Accessed: Aug. 20, 2024. [Online]. Available: https://onlinelibrary-wiley-com.proxy.lib.uwaterloo.ca/doi/full/10.1002/fuce.201700187

[3] Y. Yan, R. Bateni, J. Harris, and O. Kesler, "Fabrication of reactive element oxide coatings on porous ferritic stainless steel for use in metal-supported solid oxide fuel cells," *Surf. Coat. Technol.*, vol. 272, pp. 415–427, Jun. 2015, doi: 10.1016/j.surfcoat.2015.03.041.

[4] J. Harris, Y. Yan, R. Bateni, and O. Kesler, "Degradation of La0.6Sr0.4Co0.2Fe0.8O3—Ce0.8Sm0.2O1.9 Cathodes on Coated and Uncoated Porous Metal Supports," *Fuel Cells*, vol. 16, no. 3, pp. 319–329, 2016, doi: 10.1002/fuce.201500139.

[5] S. Molin, B. Kusz, M. Gazda, and P. Jasinski, "Evaluation of porous 430L stainless steel for SOFC operation at intermediate temperatures," *J. Power Sources*, vol. 181, no. 1, pp. 31–37, Jun. 2008, doi: 10.1016/j.jpowsour.2007.10.009.

[6] E. Mercadelli, A. Gondolini, P. Pinasco, and A. Sanson, "Stainless steel porous substrates produced by tape casting," *Met. Mater. Int.*, vol. 23, no. 1, pp. 184–192, Jan. 2017, doi: 10.1007/s12540-017-6336-2.

[7] RE Mistler and ER Twiname, "Tape Casting Theory and Practice," *Am. Ceram. Soc*, 2000.

[8] John L. Park, *Manufacture of Ceramics*. 1954.

[9] A. Kristoffersson and E. Carlström, "Tape casting of alumina in water with an acrylic latex binder," *J. Eur. Ceram. Soc.*, vol. 17, no. 2, pp. 289–297, Jan. 1997, doi: 10.1016/S0955-2219(96)00143-4.

[10] M. Boaro, J. M. Vohs, and R. J. Gorte, "Synthesis of Highly Porous Yttria-Stabilized Zirconia by Tape-Casting Methods," *J. Am. Ceram. Soc.*, vol. 86, no. 3, pp. 395–400, 2003, doi: 10.1111/j.1151-2916.2003.tb03311.x.

[11] T. C. Metcalfe, "Development and Characterization of Nickel and Yttria-stabilized Zirconia Anodes for Metal-Supported Solid Oxide Fuel Cells Fabricated by Atmospheric Plasma Spraying," 2024. Accessed: Aug. 20, 2024. [Online]. Available: https://library-archives.canada.ca/eng/services/services-libraries/theses/Pages/item.aspx?idNumber=1033054242

[12] D. Hotza and P. Greil, "Review: aqueous tape casting of ceramic powders," *Mater. Sci. Eng. A*, vol. 202, no. 1, pp. 206–217, Nov. 1995, doi: 10.1016/0921-5093(95)09785-6.

[13] C.-L. Chang, C.-H. Tsai, C.-Y. Fu, C.-S. Yang, S.-F. Yang, and R.-Y. Lee, "Fabrication and Characterization of Metal-Supported Solid Oxide Fuel Cell Fabricated by Atmospheric Plasma Spraying," *ECS Trans.*, vol. 91, no. 1, p. 855, Jul. 2019, doi: 10.1149/09101.0855ecst.

[14] M. Rauscher, G. Besendoerfer, and A. Roosen, "Steel-sheet fabrication by tape casting," *Int. J. Powder Metall.*, vol. 44, pp. 39–48, Nov. 2008.

[15] U. Scheithauer, E. Schwarzer, C. Otto, T. Slawik, T. Moritz, and A. Michaelis, "Ceramic and Metal-Ceramic Components with Graded Microstructure," in *Advanced and Refractory Ceramics for Energy Conservation and Efficiency*, John Wiley & Sons, Ltd, 2016, pp. 149–160. Accessed: Aug. 20, 2024. [Online]. Available: https://onlinelibrary.wiley.com/doi/abs/10.1002/9781119234593.ch15

[16] J. J. Abbott, "Parametric design of tri-axial nested Helmholtz coils," *Rev. Sci. Instrum.*, vol. 86, no. 5, p. 054701, May 2015, doi: 10.1063/1.4919400.

[17] Roberto Scataglini, Ahmad Mayyas *et al.*, "A Total Cost of Ownership Model for Solid Oxide Fuel Cells in Combined Heat and Power and Power- Only Applications," ERNEST ORLANDO LAWRENCE BERKELEY NATIONAL LABORATORY, U.S. Department of Energy, Office of Energy Efficiency and Renewable Energy (EERE) Fuel Cells Technologies Office (FCTO) under Lawrence Berkeley National Laboratory, Technical Report, Dec. 2015.

[18] C. Houchins, B. James, and Strategic Analysis, "Hydrogen Storage Cost Analysis," [Online]. Available: https://www.hydrogen.energy.gov/docs/hydrogenprogramlibraries/pdfs/review22/st235_houchins_2022_p-pdf.pdf?Status=Master